STEADY STATE MODELING AND ANALYSIS OF A DE-COUPLED FUEL CELL - GAS TURBINE HYBRID FOR CLEAN POWER PRODUCTION

By

GARRETT SCOTT HEDBERG

A thesis submitted in partial fulfillment of
the requirements for the degree of

MASTER OF SCIENCE IN MECHANICAL ENGINEERING

WASHINGTON STATE UNIVERSITY
School of Mechanical and Materials Engineering

MAY 2017

To the Faculty of Washington State University:

The members of the Committee appointed to examine the thesis of GARRETT SCOTT HEDBERG find it satisfactory and recommend that it be accepted.

_____
Dustin McLarty, Ph.D., Chair

_____
Cecilia Richards, Ph.D.

_____
Jacob W. Leachman, Ph.D.

ACKNOWLEDGEMENT

Wow, I guess I do not know where to begin. There is so many people to thank and give credit to for this work. I could not have done it alone. First, I must thank my family Scott, Chris, Madi and Justin. You guys have been the rock for which I could stand on and have always encouraged and pushed me to be the best person I can be. Thank you for always being there, even if you were 1500 miles away. I love you guys. Next, I want to thank my advisor, Dr. Dustin McLarty. I remember you outlining this idea on the first day I arrived in Washington. We weren't sure what results we were going to get, but I'd say it worked out well right? Thank you for continuing to push me even when I thought we had reached the finish line. I want to thank you also for taking a chance on me when you were just starting your own career at WSU. Even though a Ph.D. wasn't what I decided on you were still supportive of my choice and a constant source of information for the endless questions I asked figuring out the dFC-GT. You were a great advisor and I can't wait to see the results that start pouring out of the lab. Speaking of, I should thank everyone in the CESI lab at WSU: Nate, Nadia, Kevin, Marshall, Haley, Jeff, Ashley and Nathanael. You all definitely made coming to work so much more fun and enjoyable, while also being awesome coworkers and answering my basic MatLab© syntax questions. Thanks, and I can't wait to see what the future holds for you all! I want to give some final shout outs to my friends in Washington, Minnesota, and wherever else you may be. It's hard to accomplish anything alone, and knowing there's friends like you in my corner allowed me to continue forward even when I wasn't sure where I was going.

STEADY STATE MODELING AND ANALYSIS OF A DE-COUPLED FUEL CELL GAS TURBINE FOR CLEAN POWER PRODUCTION

Abstract

by Garrett Scott Hedberg, M.S.
Washington State University
May 2017

Chair: Dustin McLarty

This thesis introduces a de-coupled fuel cell-gas turbine hybrid arrangement that removes the fuel cell stack from the turbine working fluid, retains the high efficiency thermal integration of a topping cycle, and does not employ the high temperature heat exchangers of a bottoming cycle. The distinguishing feature of the system is the solid-state oxygen transport membrane used to create a secondary oxidant stream without significantly affecting turbomachinery performance. The secondary oxidant stream is re-pressurized and diverted to a solid oxide fuel cell. Excess hydrogen from the fuel cell supplies the combustor, which heats the oxygen-depleted air and drives the turbomachinery. The fuel cell operates in a thermally sustaining condition with direct and indirect fuel reforming providing the thermal management. Thermodynamic models developed in the Clean Energy Systems Integration Lab (CESI) at Washington State University identified the design conditions and characterized the system performance within the design space. Analysis indicates greater than 75% fuel-to-electric efficiency is achievable, with higher efficiency possible through co-production of hydrogen. The

potential to retrofit existing turbine systems, particularly micro-turbines and stand-by ‘peaker’ plants, with minimal impact to compressor stability or transient response is a promising pathway to hybrid fuel cell/turbine development that does not require bespoke turbomachinery design. Economic analysis of the developed system showed its potential to compete in the power energy market as an alternative power generation device.

TABLE OF CONTENTS

Page

LIST OF FIGURES Page

LIST OF TABLES Page

1. Introduction

The world's energy systems are undergoing radical transformation from a world in which cheap, easily extractable energy was abundant, and into the modern reality of constrained resources. New technologies are facilitating this transition, albeit at considerable economic cost. These costs are justified by air quality, climate and nuclear proliferation concerns. Energy efficiency has accommodated much of the growth in developed economies over the past 30 years, but traditional combustion based technologies are reaching the limit of feasible performance, and alternatives are desperately needed. Renewable power generation provides a cost alternative, but without dispatchable power sources to accommodate them, new installations will stall.

Uncertain fuel costs, dependence on foreign sources, public policy, and environmental concerns weigh decisively in decisions to implement new technologies into the energy infrastructure. Many established technologies have been driven to obsolescence, i.e. coal. Short-term costs have discouraged some alternatives despite long-term benefits. Early de-commissioning and replacement of existing energy infrastructure with renewable energy production and battery storage technology could prove vastly expensive, and unsustainable. A viable path towards sustainability must employ an all-of-the-above approach to energy production with an emphasis on systems that are tenable on the timescale of most power plants.

One of the technologies within the solution mix is electrochemical power production with fuel cells. The idea proposed within this thesis upgrades an existing power generation system – a gas turbine (GT) – by hybridization with a solid-oxide fuel cell (SOFC).

Fuel cells have become a staple in the alternative energy sector over the last few decades with extensive studies supporting and demonstrating high efficiency and low emissions. Fuel cells have been used to power multi-watt devices as small as laptop computers and multi-megawatt buildings as large as hospitals [*1*,*2*]. Solid oxide and molten carbonate (MCFC) fuel cells have been employed for combined heat and power generation [*3*]. SOFC's are preferred due to their completely solid state design, manufacturability, higher efficiency and ability for systems to make use of their exhausted waste heat. As stand-alone systems, SOFC generators have demonstrated fuel-to-electric efficiencies greater than 60% at sizes ranging from 1kW to many hundreds of kW.

Unlike PEM fuel cells, which operate on pure H_2, SOFC operate at high temperatures, greater than 700°C, and are thus able to operate on a variety of fuels including natural gas, landfill gas, waste gas, and logistic fuels. Operation on these fuels results in a significant concentration of CO2 in the product stream, which prevents complete utilization of the fuel via recirculation. In stand-alone systems, this unused potential energy is combusted and used to pre-heat the incoming streams. There is potential for improved efficiency by utilizing this unused fuel and any high-quality waste heat in a heat engine. By incorporating solid oxide fuel cells into gas turbine designs, the total system efficiency increases significantly from 60% to 75% fuel-to-electric (FTE) efficiency for intermediate sized systems [*4*,*5*].

Theoretical studies of FC-GT hybrids were first conducted in the early 1990's, assessing the feasibility of such systems [*6*]. The literature involving the two-system hybridization is extensive. Most systems designs are reliant on the scale of the application. For sub-MW applications, the literature tends to focus more on simple and cheap ways to combine the two

systems [*7*]. Large-scale applications – such as power generation – focus more on the efficiency, fuel costs and net power output of the system [*8*]. Two configurations are discussed in literature: the bottoming cycle and topping cycle. Each rely on the positioning of the fuel cell in the hybrid system. The bottoming cycle places the fuel cell downstream of the turbine, and utilizes the turbine's waste heat for preheating of the SOFC. Alternatively, a topping cycle places a fuel cell upstream of the turbine in a pressurized environment. The benefits of a topping cycle include i) pressurization of the SOFC which raises power production or efficiency, ii) waste heat recovery of the fuel cell displacing fuel supplied to the turbine, iii) avoidance of high temperature heat exchangers. The topping cycle introduces challenges, specifically maintaining thermal tolerances of the SOFC under changing load or degradation, and avoiding surge/stall of the compressor during transient operation.

The dFC-GT is a new topping cycle system configuration that removes the SOFC from the working fluid of the gas turbine. The de-coupled system has the potential to mitigate surge/stall during transient operation, expand the operating envelope of the hybrid system, and allow for the possibility of drop-in upgrades of existing turbine hardware. De-coupling is accomplished through the introduction of an oxygen transport membrane (OTM) that separates the compressed air into a high purity oxidant stream for the fuel cell and a depleted oxidant stream for the turbine. By removing the fuel cell from the working fluid of the gas turbine, the system is separated into two quasi-independent power generating devices (fuel cell and gas turbine) that when working harmoniously complement each other's best characteristics. The fuel cell would thus require the turbine operation, as it provides the supply of oxidant, but the turbine could still

operate independently. When both systems are operating the fuel cell waste energy displaces the fuel to the turbine, thus improving efficiency.

The physical linkage between the systems remains only in the form of an oxidant stream and a fuel byproduct stream, either of which can be stored, diverted, or substituted during transient or off-design operations. The system retains the thermodynamic coupling common to most topping cycle FC-GT systems which benefit from the following:

- Electrochemical conversion of the fuel prior to any combustion
- Reduced parasitic losses of air compression
- Increased net efficiency with electrical output from both systems
- Pressurization of the fuel cell.

In addition to the above benefits, the dFC-GT improves upon previous hybrids by:

- De-coupled design; i.e. limiting potential downfalls of FC-GT arrangements
- Retro-fit capability; i.e. no bespoke turbomachinery development
- Increased hydrogen co-production potential

1.1. Thesis Outline

The goal of this study is the evaluation and characterization of the dFC-GT hybrid concept. To achieve this goal a detailed thermodynamic study was undertaken with the following objectives:

Objective 1) Model steady-state operation of a dFC-GT hybrid using fundamental thermodynamic and electrochemistry principles.

Objective 2) Characterize nominal operation and the scope of the feasible operation envelope.

Objective 3) Identify challenges and beneficial attributes of the dFC-GT hybrid, specifically in regards to retro-fit feasibility, hydrogen recovery, and compatibility with low pressure ratio micro-turbines.

Objective 4) Perform a sensitivity analysis to identify critical design trade-offs of the system.

Objective 5) Investigate the economic feasibility of the dFC-GT system.

To accomplish these goals all components and modeling assumptions will be expanded upon. Chapter 2 gives an overview of all components used in the system presented, e.g. fuel cells, gas turbines, heat exchangers, and OTM's. Chapter 3 reviews the relevant literature for fuel cell gas turbine hybrids, setting the stage for the proposed technology improvement.

Chapter 4 introduces the modeling considerations and the underlying thermodynamic analysis underpinning the system models. Chapter 5 details steady state results, demonstrating how the de-coupled system works as a retrofit technology that improves upon the FC-GT concept. Chapter 5 also introduces the application of this technology to micro-turbines and hydrogen co-generation.

Further discussion on economics, and feasibility of dFC-GT will be presented in Chapter 6. Annual operating costs and carbon emissions will be the driving variables for the analysis. Finally, Chapters 7 and 8 will give an outlook for the de-coupled FC-GT.

2. Background

2.1. Fuel Cells:

A fuel cell is an electrochemical conversion device that can convert chemical energy to electrical and thermal energy by means of electrochemical reactions within the cell. Fuel cells are not batteries, meaning they do not store energy, but rather require a continuous source of fuel to sustain electricity production. Fuel cells are also not thermal engines, and thus do not abide by the Carnot limit common to all thermal engines. This enables fuel cells to be highly efficient conversion devices.

The concept of energy conversion through chemical means was discovered in 1838 when Sir William Robert Groves [*9*,*10*] combined hydrogen and oxygen electrochemically to produce an electric load. Groves realized that a constant current would flow between platinum electrodes he had immersed in sulfuric acid. He then sealed the other end of the plates in hydrogen and oxygen respectively (Figure 1).

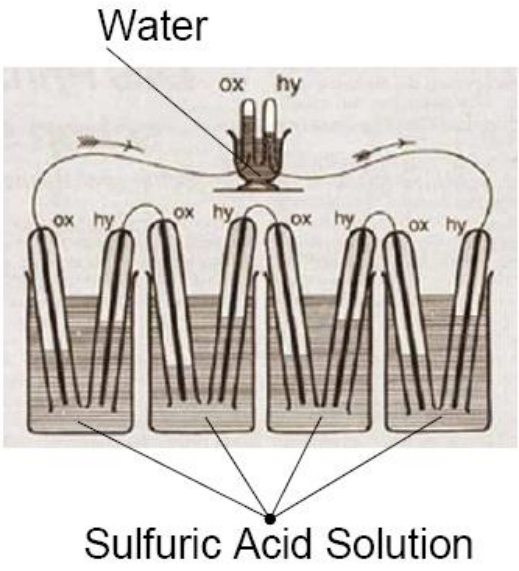

Figure 1" Gas Battery" Concept by William Groves [10]

As electrons were passed along the interlaying wire, the liquid levels within the chambers would rise and fall. By seeing the liquid levels change, Groves realized the gases were reacting with a constant current, and by placing many of these devices in series Groves created the "Gas Battery." Now known by all as the fuel cell.

2.1.1.Fuel Cell Structure

To understand the physics and mechanics of the fuel cell it is necessary to examine the components, designs, and reactions of the device.

There are three layers in all fuel cell types.

- Anode – a porous electrode where oxidation reactions occur;
- Cathode – a porous electrode where reduction reactions occur;
- Electrolyte – ionically conductive, but not electrically conductive, dense material that separates the anode and cathode [*11*]

Figure 2 depicts a typical fuel cell structure. Electrolyte types are the governing classification for fuel cells.

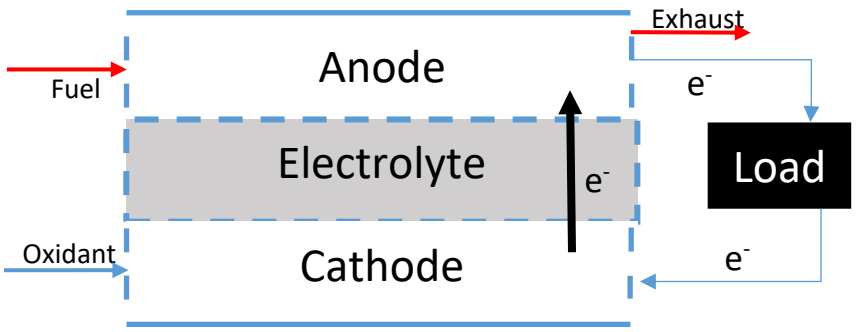

Figure 2 Basic Fuel Cell Assembly

Fuel cells work by separating electrons from a fuel source and forcing them to travel through a circuit, generating electric power. A fuel cell operates continuously so long as the necessary fuel and oxidant flows are sustained and the reactant is consumed and replenished.

The governing reaction within a hydrogen/oxygen fuel cell, is:

$$H_2 + \frac{1}{2}O_2 \leftrightharpoons H_2O \qquad (1)$$

In this type of fuel cell two electrochemical half reactions occur at the anode (2) and the cathode (3) site. In the specific case of SOFC the half reactions are as follows:

$$2H_2 + 2O_2 - \leftrightharpoons\ 2\mathrm{H_2O} + 4e^- \qquad (2)$$

$$O_2 + 4e^- \leftrightharpoons 2O_{2-} \qquad (3)$$

Separation of these reactions allows for the electron transfer from the fuel though the external circuit before completing the reaction.

2.1.1.Steam Reformation

Steam reformation is an endothermic reaction that produces hydrogen, carbon monoxide, and other useful products from hydrocarbon fuels. Steam reformation is utilized in fuel cell systems to reform a fuel and produce hydrogen for the cell stack. This is accomplished externally through a reformer [*12*] or, in the case of the dFC-GT, the steam reformation internally balances the heat generated in the fuel cell (Figure 3). For the purposes of this study steam-to-methane (SMR) will be considered at a constant steam-to-carbon (S2C) ratio.

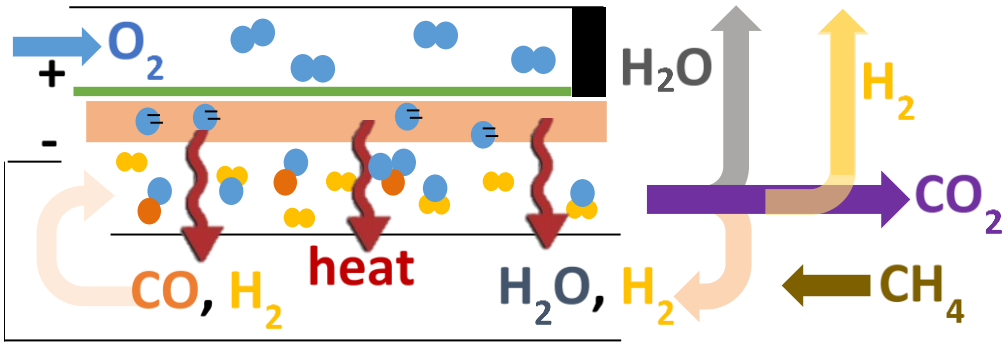

Figure 3 Internal Reformation Concept ([30])

The reforming of CH_4 is easily integrated into fuel cell systems. At high temperatures and in the presence of metal-based catalysts, steam will react with methane to yield carbon monoxide (CO) and hydrogen (H_2).

$$CH_4 + H_2O \leftrightharpoons CO + 3H_2 \quad (4)$$

Additional hydrogen is produced by the water-gas shift reaction (5). The reaction kinetics of water-gas-shift are much faster than steam reforming, and it can generally be assumed that CO and CO2 are in equilibrium always.

$$CO + H_2O \leftrightharpoons CO_2 + H_2 \quad (5)$$

2.1.2.Fuel Cell Types

Fuel cell types are governed by the type of electrolyte each utilizes. Common fuel cell types are polymer electrolyte fuel cells (PEM), molten carbonate fuel cells (MCFC), and solid oxide fuel cells (SOFC). Each type has advantages and disadvantages specific to their typing. PEM fuel cells, for example, are beneficial to automobile applications for their high-power density and low temperature operating ranges (60-80 C) [*11*,*4*]. Both the MCFC and SOFC operate in higher temperature ranges. Higher operating temperatures eliminate the use of noble metals to act as catalysts within the fuel cell and thus reduce cost of the system. Due to these high operating temperatures, many proposed designs exist to combine SOFC's and MCFC's with heat engine systems to raise net efficiency. Molten carbonate cells operate between temperatures of 600-800^{o}C, while solid oxide fuel cells operate between temperatures of 700-1000^{o}C. At these temperatures exhaust products contain sufficient thermal energy that can be recycled and reused to further improve efficiencies.

2.1.3.Solid Oxide Fuel Cells (SOFC)

Solid oxide fuel cells are a high temperature class of cell that employ a thin ceramic membrane as an electrolyte. Oxygen ions (O^-) are the ionic charges carried across the SOFC membrane and responsible for the half reactions at the anode and cathode. The ceramic electrolyte is commonly made of two types of ceramic, Yttrian stabilized zirconia (YSZ) or gadolinium doped ceria (GDC) [*13*]. Both operate as oxygen vacancy materials and are

sufficient to handle a variety of temperature ranges including the high operating temperatures of SOFC's.

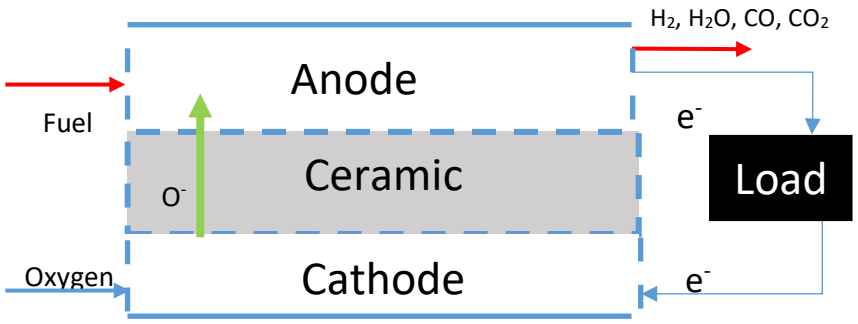

Figure 4 SOFC Structure

Figure 3 shows a schematic of a typical SOFC. Reactions occur at the boundaries of the anode and cathode with the electrolyte. At the cathode, the incoming oxidant enters and draws electrons from the electrolyte to form oxygen ions (O-). The resulting ions are transported across the electrolyte to the anode side of the fuel cell. At the anode, high temperatures can reform fuel to obtain hydrogen. This incoming hydrogen reacts to the oxygen present at the electrolyte. Oxygen ions are drawn out to form water and electrons are released at the anode. These electrons are then forced through an external circuit generating electricity and sending electrons back to the cathode side of the cell.

The high operating temperatures of SOFC's provide both advantages and disadvantages. [*5*,*11*,*14*,*15*]. Advantages of SOFC's include fuel flexibility, allowing the cell to work with many different types of fuels including natural gas, methanol, and formic acid. Disadvantages include problematic material issues associated with very high operating temperatures. This includes cracking of the ceramic electrolyte, long start-up times, and sealing issues.

2.1.4.Thermodynamics of Fuel Cells

Operation of fuel cells is heavily dependent on an understanding of thermodynamic phenomena happening within the cell assembly. This section will be a brief overview on cell thermodynamics and the governing equations that will be significant in the modeling of the final system in Chapter 5.

The most important fuel cell parameters during the operation of the system are changes in the enthalpy and Gibbs free energy of the cell. Equation 6 represents the enthalpy balance for a chemical reaction.

$$\Delta H_{RXN} = \sum_{PROD} \gamma_{PROD} h_{f,PROD} - \sum_{REACT} \gamma_{REACT} h_{f,REACT} \quad (6)$$

Where subscripts *PROD* and *REACT* correspond to the reactions products and reactants, and:

h_f = enthalpy of formation

γ = Stoichiometric coefficient for each component

Equation 7 describes the hydrogen/oxygen fuel cell reaction in terms of standard enthalpies of formation (^{0}). Taken at 1 atm and 298 K, this results in a reaction enthalpy of -285.83 kJ/kmol.

$$\Delta H^0_{H_2+\frac{1}{2}O_2 \rightarrow H_2O} = 1h^0_{f,H_2O} - (1h^0_{f,H_2} + \frac{1}{2}h^0_{f,O_2}) \quad (7)$$

The change in Gibbs free energy of reaction determines the ideal open circuit potential of the reaction. Equation 8 presents the balanced Oxygen and Hydrogen reaction, while equations 9 and 10 relates this to the voltage potential, E.

$$\Delta G^0_{RXN} = 1G^0_{f,H_2O} - (1G^0_{f,H_2} + \frac{1}{2}G^0_{f,O_2}) \quad (8)$$

$$\Delta G = -W_{EL} \quad (9)$$

$$W_{EL} = Q \cdot E \quad (10)$$

The charge, Q, can be used to relate the total energy to the moles of reactants through Faraday's constant and the electrons per reaction, n, in equation 11. This derivation is summed up by the energy balance of equation 12 relating the Gibbs energy to the open circuit voltage of the reaction. For a hydrogen – oxygen reaction at STP, this voltage is 1.23 Volts.

$$Q = n \cdot F \tag{11}$$

$$\Delta G = -nFE \; or \; E^0 = -\frac{\Delta G}{nF} \tag{12}$$

The Nernst equation relates this reaction voltage to that which would be seen in a fuel cell operating at conditions other than STP. Beginning with Van't Hoff's formula, equation 13, and assuming the change in enthalpy is independent of temperature, the derivative with respect to temperature becomes equation 14. Substituting for Gibbs energy with equation 12, this can be re-written as equation 15.

$$\Delta G = \Delta H - T\Delta S \tag{13}$$

$$\frac{d(\Delta G)}{dT} = -\Delta S \tag{14}$$

$$\frac{d(-nFE)}{dT} = -\Delta S \tag{15}$$

Transforming and integrating this differential equation leads to the Nernst equation dependent on temperature:

$$E_T = E^0 + \frac{\Delta S}{nF}(T - T^0) \tag{16}$$

To consider the composition effects on voltage chemical potentials of reactants and products must also be considered.

$$\mu_i^{\alpha} = \left(\frac{\delta G}{\delta n_i}\right)_{T,P,n_{j\neq i}} \quad (17)$$

Where μ_i^{α} is the chemical potential of species *i* in phase α and $(\frac{\delta G}{\delta n_i})_{T,P,n_{j\neq i}}$ shows how much Gibbs free energy of the system changes for an infinitesimal change in the quantity of species *i*. It is important to note that this equation holds temperature, pressure, and any quantities of another species constant. The chemical potential can be related to concentrations through the activity *a*

$$\mu_i = \mu_i^0 + RTln(a_i) \quad (18)$$

The activity *a* is a function of partial pressures p_i and p^0 where p_i is the partial pressure of the gas, and p^0 is the standard-state pressure (1 atm). Equations 17 and 18 are combined into equation 19 and re-arranged into 20 using equation 12.

$$dG = \sum_i \mu_i dn_i = \sum_i [\mu_i^0 + RTln(a_i)] \cdot dn_i \quad (19)$$

$$E = E^0 - \frac{RT}{nF} \ln \left[\frac{\prod a_{prod}^{v_i}}{\prod a_{react}^{v_i}}\right] \quad (20)$$

Equation 20 is known as the Nernst equation. The Nernst equation outlines how the reversible cell voltage varies as a function of species concentrations, gas pressures, etc. Using the knowledge that activity is a function of partial pressures, and partial pressures are in turn a function of component concentrations, the Nernst potential for a Hydrogen/Oxygen reaction can be rewritten as equation 20, illustrating how the fuel cell operating voltage is dependent on the temperature, pressure, and concentrations all present within the cell stack.

$$E = E^0 - \frac{RT}{nF} \ln \left[\frac{X_{H_2O}}{X_{H_2} \cdot X_{O_2}^{\frac{1}{2}}}\right] \quad (21)$$

2.1.5.Fuel Cell Losses

Fuel cell power output depends on the operating voltage and operating current. A fuel cell can be characterized by a set of j-V curves representing cell performances at different operating temperatures or fuel concentrations [*16*]. These charts are often normalized by area to better compare button cell tests to commercial scale cells. The open circuit potential, or OCV, given by equation 21, represents the maximum voltage when no current is drawn. The shape of j-V curves for fuel cells depends on the fuel cell reversible voltage and losses that occur during operation at certain current density and voltage levels.

Three main types of losses are discussed throughout literature [*16*].

- Activation losses (mainly influencing cells at lower current densities).
- Ohmic losses (resulting in resistance across the electrolyte).
- Concentration losses (occurring at higher current densities).

Initiating the electrochemical reaction requires a certain input of energy. This "activation" energy corresponds to the barrier that must be overcome before the main reaction proceeds. Ohmic losses are associated with the innate resistance of the material the electrolyte is manufactured from. The final type of loss is concentration losses. These losses occur from the restrictions on the transport of gases to the anode or cathode [*16*]. These losses typically occur when the rate of fuel consumption is higher than diffusion. Local starvation of fuel at the reaction sites reduces the activity and leads to a net output voltage loss.

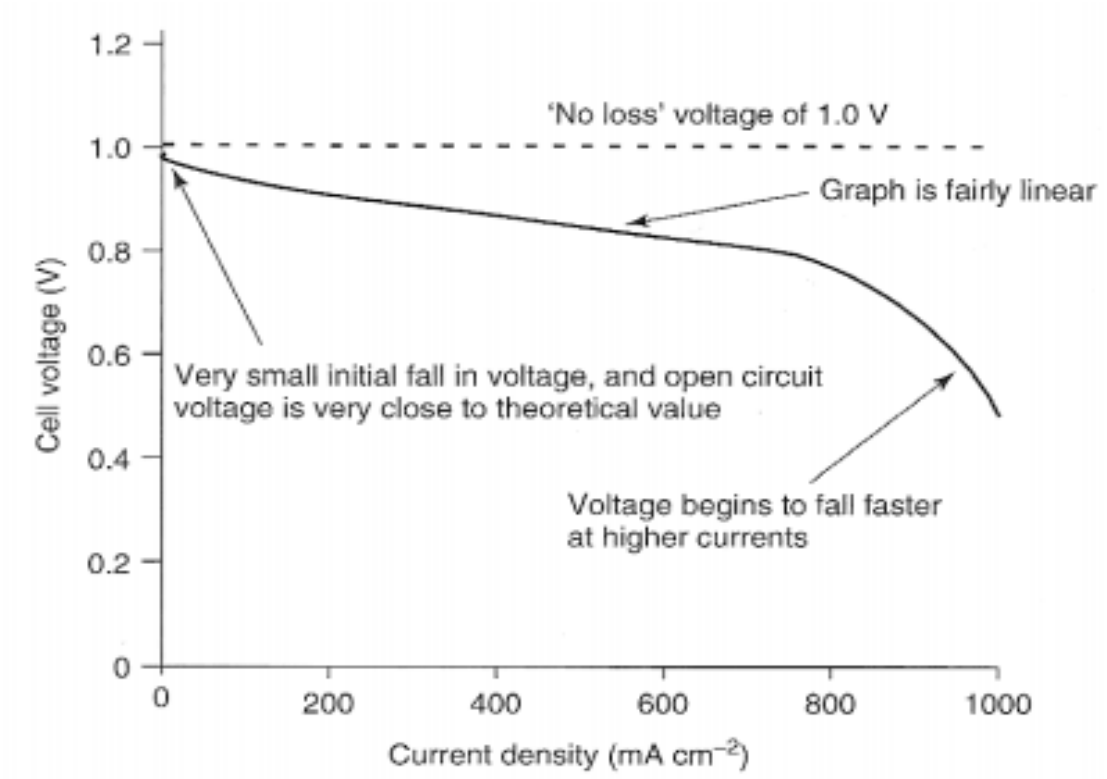

Figure 5 Fuel Cell Losses [31]

Figure 5 shows a typical j-V curve of a fuel cell. The dotted horizontal line shows an ideal open circuit potential (for this example we will assume it is 1 Volt). The solid curved line is the operating line of a fuel cell. Notice that at 0 current density the actual cell voltage does not equal the open circuit potential. This is due to the initial activation loss common to all cells. As the current density increases, the cell voltage falls nearly linearly due to resistances of the electrolyte. At high current densities, the voltage falls rather quickly due to the concentration losses.

The combination of these three losses affect the total output voltage of the fuel cell. From Figure 5 one can see that each type of loss dominates a certain region of current densities. For the rest of this thesis and the resulting steady state analysis will only consider the Ohmic loss region in the mid-current density range.

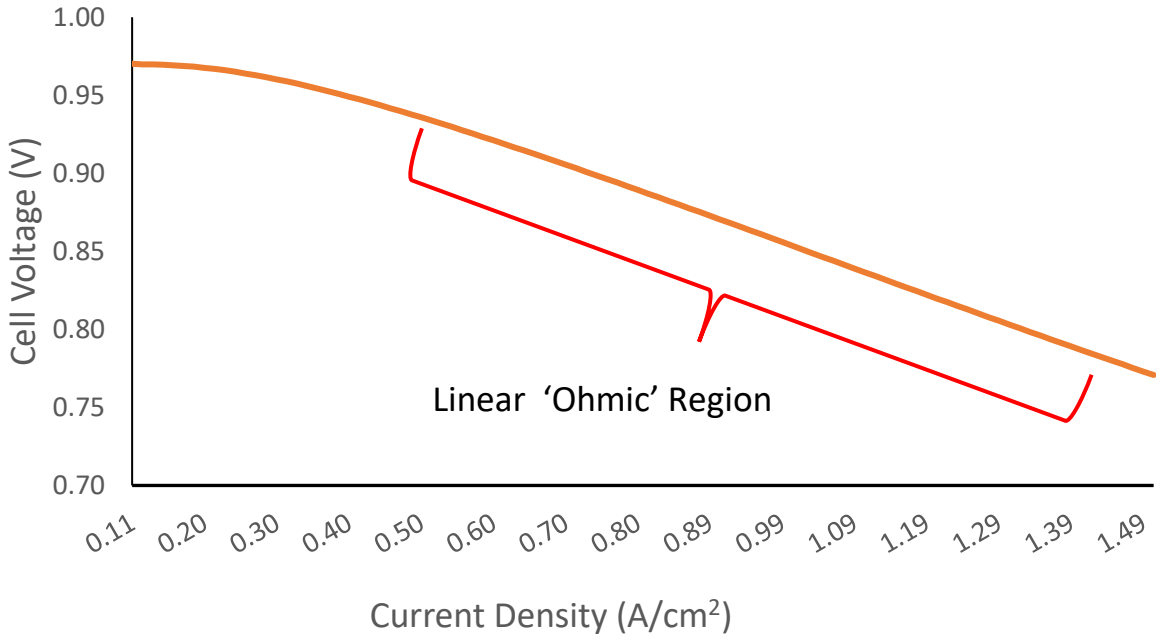

Figure 6 Ohmic Losses

Ohmic losses are caused by the electrical resistance the charge must overcome while traveling across the electrolyte. The resulting linear relationship, '*V = IR,*' is captured in the "Ohmic" region of Figure 6. Resistance across the electrolyte is a material property, and thus must be tested directly or assumed from empirical data. The standard metric for comparing resistances between fuel cells is the Area Specific Resistance (ASR). The ASR is the resistance of the electrolyte normalized by the area of the fuel cell. Using the ASR enables quick calculation of ohmic losses by multiplying ASR by the total current density of the cell.

2.2. Gas Turbines

A gas turbine is a power generating device that uses a thermodynamic cycle called the Brayton cycle, pictured in Figure 7. The ideal Brayton cycle typically consists of a compressor, a mixing chamber (combustor), and an expander (turbine). The ideal Brayton cycle operates on a four-step process, also labeled in Figure 7.

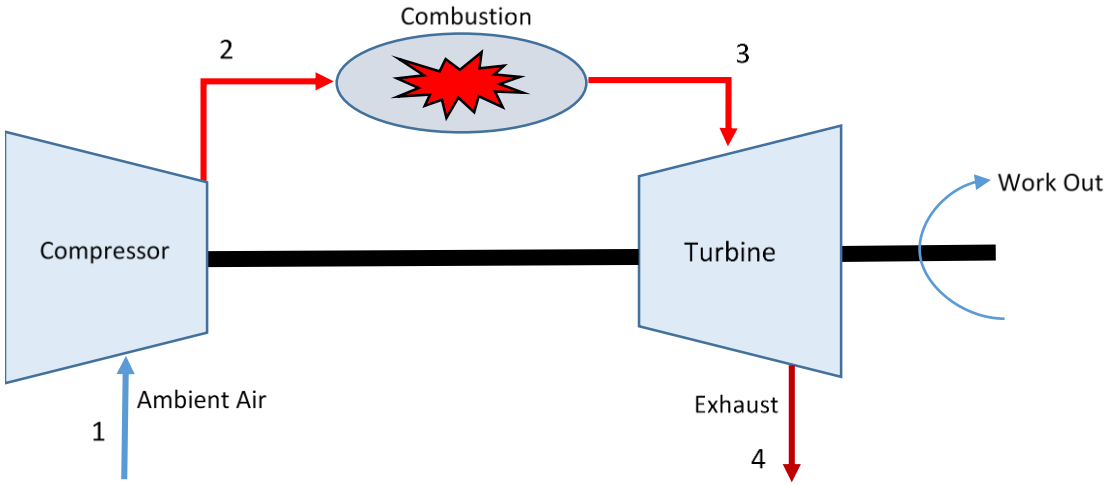

Figure 7 Simple Cycle Gas Turbine

1– 2) Isentropic Compression: Ambient fluid is drawn into the compressor and pressurized.

2 – 3) Isobaric Combustion: The fluid is ignited at constant pressure through a combustor.

3 – 4) Isentropic Expansion: The combustion process heats the air and lets it expand rapidly to the turbine.

4 – 1) Isobaric Heat Rejection: The fluid exits the turbine back to ambient conditions. The process of expansion and heat rejection spins the turbine, generating power to the compressor and some work out.

The first law efficiency of an ideal Brayton cycle can be derived simply as the work in over the heat in.

$$\eta_{Brayton} = \frac{\dot{W}_{net}}{\dot{q}_{in}} \tag{22}$$

Cold-air-standard analysis can simplify the estimation of system efficiency by making a few assumptions about the ideal Brayton cycle. Assuming constant mass flow and constant specific heats, the change in enthalpy between two states can be re-written as $\Delta H = \dot{m} \cdot C_p \cdot \Delta T$.

For the four-step process of the ideal Brayton cycle listed above, one can now the efficiency of the Brayton cycle as:

$$\eta_{Brayton} = \frac{c_p(T_{combustor\ out} - T_{turbine\ out}) - c_p(T_{compressor\ out} - T_{air})}{c_p(T_{combustor\ out} - T_{combustor\ in})} = \frac{c_p(T_3 - T_4) - c_p(T_2 - T_1)}{c_p(T_3 - T_2)} \quad (25)$$

This equation can be simplified further to:

$$\eta_{Brayton} = 1 - \frac{(T_1 - T_4)}{(T_3 - T_2)} \quad (26)$$

Applying the isentropic relation (27), the Brayton cycle efficiency can be simplified to a simple function of the pressure ratio (28). This calculation of cycle efficiency becomes more complicated when realistic efficiencies are considered for the compressor and turbine.

$$\frac{T_{in}}{T_{out}} = \left(\frac{P_{in}}{P_{out}}\right)^{\left(\frac{\gamma-1}{\gamma}\right)} \quad (27)$$

$$\eta = 1 - \left(\frac{P_{In}}{P_{Out}}\right)^{\left(\frac{\gamma-1}{\gamma}\right)} \quad (28)$$

2.3. Heat Exchangers

Heat exchangers are widely used engineering devices that transfer heat between one or more fluids. These fluids can be in direct contact, or separated by a barrier to prevent mixing. Heat exchangers are employed in gas turbine and/or fuel cell systems to either lower the temperature of a fluid as it enters a component, or pre-heat the fluid as it enters the component.

Heat exchangers are classified by their flow arrangements. In a parallel-flow arrangement, two or more fluids enter the same side of the heat exchanger and transfer heat as they flow parallel to each other. Counter-flow heat exchangers have two or more fluids enter at opposite ends of the component, and exchange while flowing opposite each other. Cross-flow exchangers allow the fluids to enter and flow perpendicular to each other while exchanging energy. In a fuel cell gas turbine hybrid, cross flow heat exchangers enable heat recuperation to help preheat components and recycle waste heat.

2.4. Oxygen Transport Membrane

This study introduces a new component to the fuel cell gas turbine hybrid. Oxygen transport membranes are used in industry today to separate oxygen for oxy-combustion and syngas production. They are ionic transport membranes that are fabricated from mixed-conducting ceramic oxides that can conduct ions at elevated temperatures, much like a SOFC [*17*,*18*]. Oxygen transport is accomplished by the hopping of oxygen ions through vacant sites in porous materials such as perovskites [*19*,*20*] under an oxygen partial pressure driving force, as depicted in Figure 8. Oxygen transport membranes produce high purity, high flux separation of oxygen from a compressed inlet air stream [*21*,*22*].

The oxygen flux has been found to be commercially viable for production of both oxygen and syngas using partial oxidation of methane [*23*,*24*,*25*,*26*]. High purity oxygen is released from the OTM at significantly lower pressures than the inlet stream. The resulting non-permeate stream of depleted oxygen has a minimal pressure drop from the loss of concentration. Production of syngas can be accomplished by oxidizing a sweep gas on the permeate side of the membranes

[*27*]. Transport membranes have also been integrated in gas turbine systems to produce an OTM-GT hybrid [*21*,*28*]. These systems produce pure oxygen for the combustors and rely on oxy-combustion.

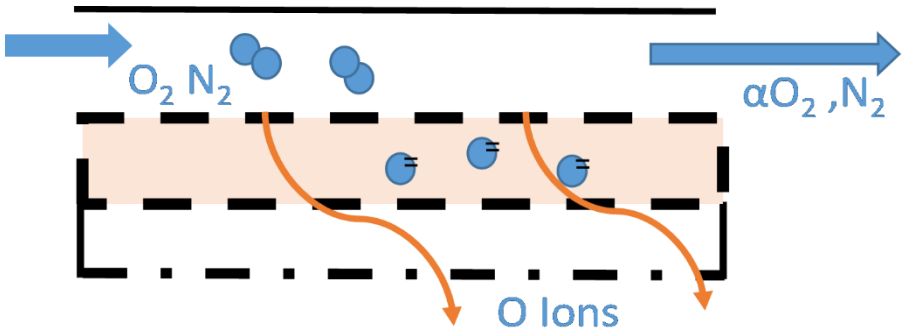

Figure 8 Praxair Oxygen Transport Membrane

Problems in transport membranes have arisen from degradation of the permeate side of the membrane due to tainted sweep gases and pressure gradients damaging the membranes over time. Introduction of transport membranes into a gas turbine system lead to rises in membrane temperature, thus degrading the membrane even faster [*29*]. Derivations of the OTM system will be presented in Chapter 4.

2.5. Hybrid Systems (FC-GT)

Hybrid systems combine two or more power generating devices and make use of the cooperation between them to maximize the power output as well as system efficiency. These systems include combined heat and power systems (CHP), hybrid vehicle engines, and the focus of this study, fuel-cell gas turbines (FC-GT).

The performance of a FC-GT hybrid systems is realized through the thermal coupling of an electrochemical generator and a classic heat engine. Fuel cells bypass the entropy generation of combustion and directly convert a fuel's stored chemical potential into electric power. Fuel cells

cannot, however, utilize 100% of the fuel provided and they generate significant heat from the inefficiencies of the electrochemical process. The hybrid arrangement utilizes this heat and waste fuel in the anode off-gas to drive the gas turbine's turbomachinery. In return, the turbine provides the air flow that sustains the electrochemistry and manages the thermal balance of the stack. In topping cycle configurations, the fuel cell is pressurized and placed immediately upstream of the combustor.

David J. White [*6*] wrote that although the inclusion of fuel cells into gas turbine-like machinery was a novel idea emerging in the early nineties, the concept would not be taken seriously until high temperature fuel cells (such as the SOFC) became commercially viable. As manufacturing costs of fuel cells have fallen, the FC-GT hybrid configuration has become an attractive option for power production.

2.5.1.De-Coupled Fuel Cell Gas Turbine

Figure 9 illustrates the configuration of a de-Coupled Fuel Cell Gas Turbine (dFC-GT). The OTM operates on a pressure differential and de-couples the fuel cell from the gas turbine by separating a portion of the oxygen from the primary air stream. It then diverts the pure oxygen feedstock to the fuel cell. The remaining oxygen depleted air is heated in the post-combustor and expanded in the turbine to drive the compressor and generate additional power. The pre-combustor is necessary to preheat the exiting compressor flow to nominal OTM operating conditions.

The OTM is more compact than the SOFC it replaces, and the impact to the primary air flow is minimal. This minimal impact enables the dFC-GT to be envisioned as a retro-fit technology. By

only interrupting the mass flow of the gas turbine through the OTM, the fuel cell may be integrated to the system with minimal risk of losing surge margin. The compressor/OTM/turbine now make up the gas turbine portion of the dFC-GT, while the SOFC becomes a separate, yet integrated power generating system.

The SOFC reforms a hydrocarbon fuel to produce hydrogen for the electrochemical reactions. This pressurized, pure oxygen fed SOFC will be referred to as the Oxy-FC, and was conceptualized by McLarty et al. [*30*]. In the standard topping cycle, waste heat from the fuel cell, supplemented by oxidation of unused hydrogen, drives the turbine. This classical FC-GT configuration replaces low efficiency heat engine combustion with heat from the fuel cell to power the heat engine.

Unlike previous hybrids, the dFC-GT recovers the fuel cell waste heat as H_2 through steam reformation of additional fuel. The resulting excess hydrogen can either be recovered as a secondary fuel product or displace fuel used to drive the turbine cycle. By replacing some or all the fuel necessary to sustain the turbine and generate power, avoiding the parasitic demands of a typical SOFC air handler and recovering fuel cell waste heat as chemical energy, the hybrid arrangement achieves remarkable performance. Power is generated by both the gas turbine and Oxy-FC.

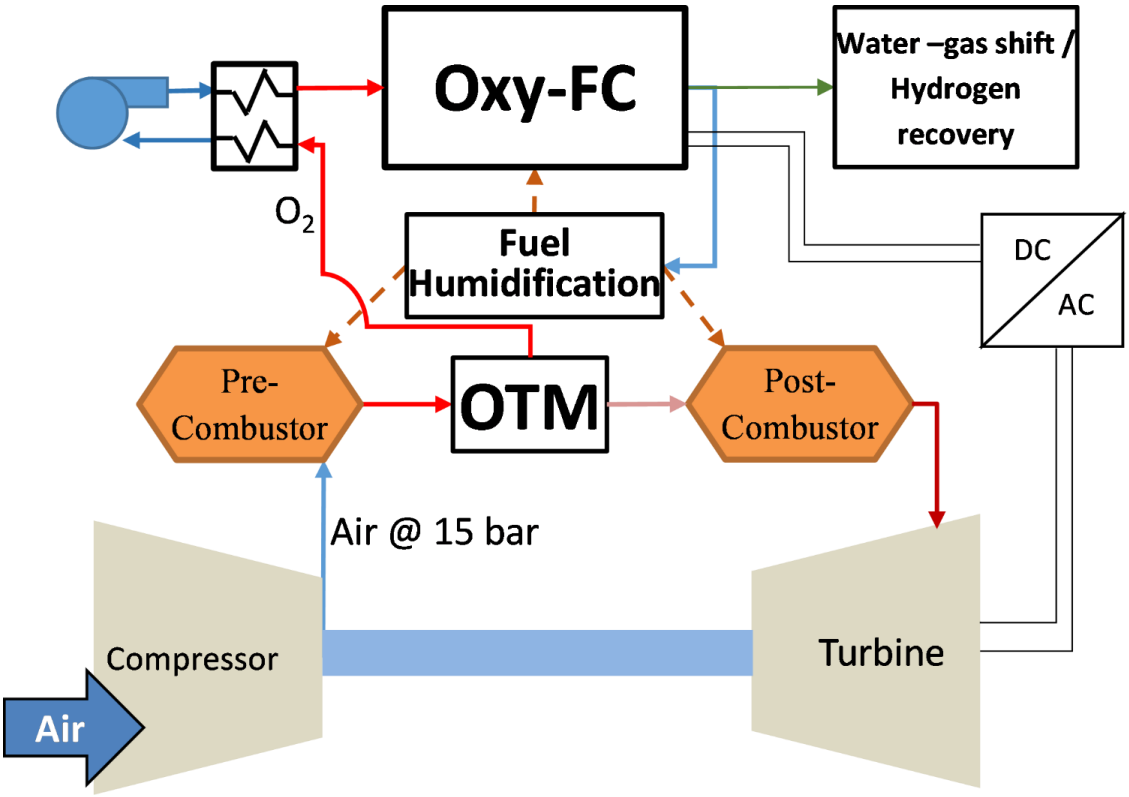

Figure 9 Schematic of de-coupled FC-GT (dFC-GT)

The dFC-GT relies on the ability of the SOFC to internally reform steam to thermally balance the system. This has been proposed by many to reduce excess equipment of high temperature heat exchangers and large blowers to recirculate air or cold by-passes to cool the fuel cell [*31*]. Real world tests of internal steam reformation for thermal balancing have not succeeded as the thermal gradients across the fuel cell are challenging to estimate and the reformation reaction cannot be controlled [*31*]. External reformation has also been investigated [*32*] but internal reformation results in better performance given the same optimal cell temperature. For this reason, this design analysis will focus on internal reformation to balance the thermal energy of the fuel cell component.

Supplying pure oxygen to the SOFC cathode increases the operating voltage and/or power density of the fuel cell [*30*]. Lower hydrogen utilizations are achieved and excess hydrogen is sent out in the exhaust of the fuel cell. This hydrogen is used to fire the turbomachinery, but may also be recirculated to help the reformation process of steam. Pressurization of the SOFC component may help the reformation reaction, but more tests need to be conducted.

The de-coupled arrangement proposed is more compatible with existing gas turbines as a retro-fit technology. Maintaining the surge margin and removing the thermal inertia of the SOFC system should retain the transient capability of a peaking generator. The fuel cell is independently controllable since the oxygen flux to the fuel cell can be independently controlled by changing the back pressure of the OTM. The de-coupled system can operate as a classic gas turbine or an advanced hybrid system as demands change.

2.6. Economics

As stated previously, the world is at a crossroads of cost and technology. Energy prices are rising yet improved technologies costs continue to fall. This dichotomy stems from the ever-evolving manufacturing processes of power systems and energy storage devices, and our insatiable desire for more and more energy. Nowhere is this clash more apparent than in California. The duck-curve [*33*], shown in Figure 10 shows the projection of energy need versus ramp up capabilities of classic gas turbine power plants in California. The cheaper prices of solar PV technology have made it a staple in the residential and commercial sectors but create deeper troughs for traditional coal and natural gas plants to ramp up in order to meet peak load demands [*34*,*35*].

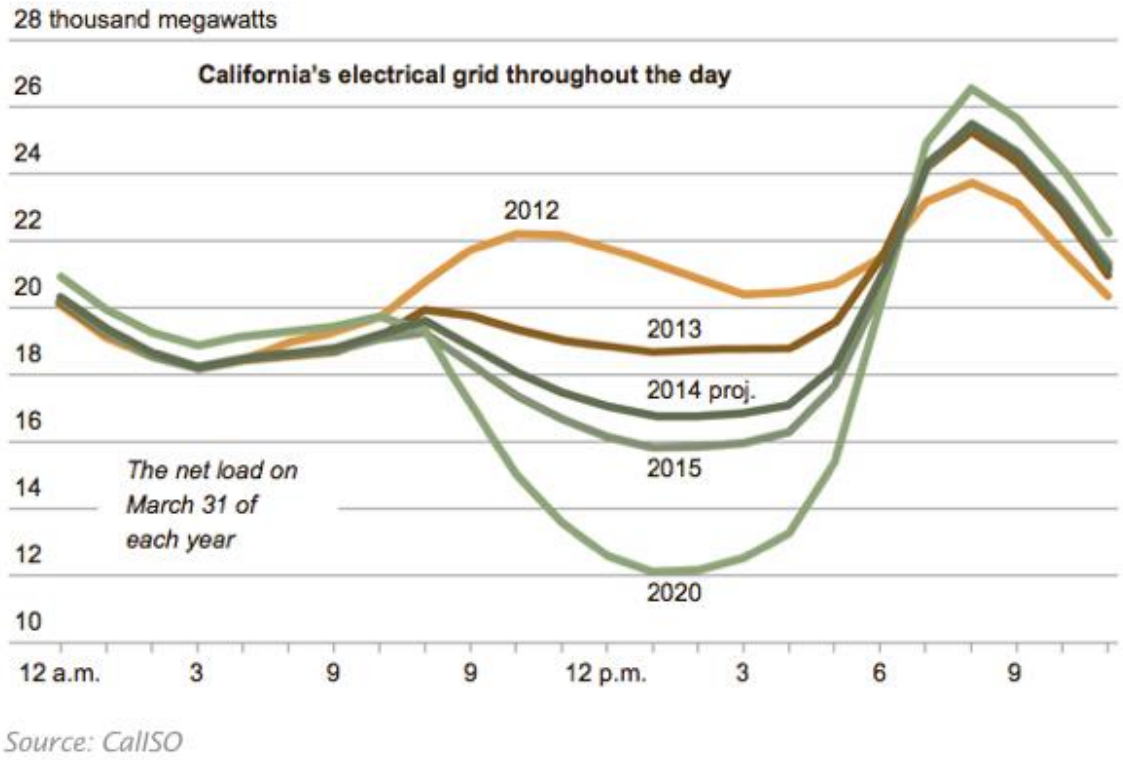

Figure 10 California's "Duck Curve" [33]

The duck curve is one example that demonstrates the need to optimize our existing infrastructure to handle the peak demands as we increase the unpredictable renewable contribution to the grid. Peak demand loads are currently met through a combination of energy storage i.e. batteries, and 'peaking' power plants [*36*]. 'Peaker' plants are fossil fuel gas turbine plants that remain in idle, but ramp up quickly to meet peak demand if the grid can't handle the load. Capital investment and cost of implementing new technology hinders the development of optimizing our energy infrastructure, therefore, the system proposed in this thesis looks to act as a retro-fit technology to 'peaking' power plants. Retro-fit power systems add components to an existing power generation device to improve either its efficiency and/or power.

Retro-fitting the generation systems already in use today not only saves in costs, but also paves a link between the fossil fuel past, and renewable fuel future. The dFC-GT demonstrates this capability in three ways:

1) By acting as a retro fit system for optimization of existing power generating gas turbines.
2) Optimizing micro-turbine efficiency for residential and/or commercial applications.
3) Providing a hydrogen generation component to further expand hydrogen infrastructure.

3. Literature Review

This chapter will give an overview of current research into SOFC and FC-GT technology. The aim of this chapter is to establish a base for which the following results and models of this thesis may stand on. Descriptions of different modeling approaches of fuel cells and hybrid configurations will help the reader understand this thesis' final model.

3.1. Modeling Approaches

Modeling has become essential in evaluating the performance and feasibility of hybrid systems. High cost of equipment and risk of destroying crucial pieces of the system have driven researchers to develop many different models for analyzing proposed systems. The most difficult model to create in a FC-GT hybrid is the SOFC. Differences in modeling rely on the desired output and configuration of the system. Current fuel cell models are capable of single-cell or multi-cell stack arrangements.

3.1.1.Fuel Cells

Bulk models (sometimes referred to as lumped models) were the first to be used in fuel cell modeling [*37*]. Bulk models do not capture any spatial variation in gas concentrations or reaction rates. Bulk models must be calibrated for a specific operating condition, and fail to capture performance under changing conditions, such as in a design study.

More detailed models rely on spatial information, concentrations, heat transfer, or mass transfer. For spatial models the fuel cell is often given a fixed size (in the design phase) or a known cell's dimensions are input to the model. Using the dimensions and breaking the cell into nodes allows for the distribution of temperature, mass, or electric parameters such as voltage and

current to be calculated along the length of a fuel cell. Palsson [*40*], McLarty [*30*], and others use these detailed models to more accurately describe the thermodynamic phenomena occurring across the fuel cell. This thesis will rely on a combination of detailed nodal model and bulk models. The nodal model will be used for a single cell analysis, while the bulk will take the single cell results and increase it to stack size for gas turbine integration.

3.1.2.Gas Turbines

Gas turbine modeling has been utilized to examine performance and efficiency of turbomachinery. Because gas turbines are widely used machines the modeling techniques governing them are relatively similar. Gas turbines operate on the Brayton thermodynamic cycle, and thus thermodynamic relations can be used to model their behavior and overall efficiency.

Chinda et al [*41*] utilized isentropic relations to model gas turbine behavior by using design pressure ratios and solving for outlet temperatures of the compressor and turbine. Solving for changes in temperatures allows for the change in enthalpies and thus total power consumed by the compressor and generated by the turbine can be calculated. Often time's initial calculations through thermodynamic relations are refined using real-world data and compressor efficiency maps. McLarty et al [*15*], in their paper on FC-GT optimization used compressor maps and normalized cathode air flow in a hybrid system to size and model optimal turbine size for a given fuel cell. This thesis will rely on steady state analysis and constant air flow to the inlet of the compressor. As such, isentropic relations will be employed to model gas turbine behavior and optimal sizing for fuel cells.

3.2. FC-GT Hybrids

Fuel cell gas turbine hybrids have been theorized by many throughout the latter part of the 1990's and into the early 2000's [*42*]. Since its inception, the hybrid FC-GT has been extensively studied and repeatedly shown its promise as an ultra-high efficiency and near-zero emission technology [*14*,*15*]. Investigations into FC-GT applications have ranged from locomotive applications [*43*], to CO_2 sequestration plants [*37*], all the way to energy production through distributed generation systems [*44*], as well as plant scale systems [*1*]. Aerospace applications for hybrid systems have also been investigated by NASA, Boeing, Airbus, and others [*45*,*46*]). FC-GT hybrids have demonstrated efficiencies as high as 56% [*47*,*48*], while proposed systems could achieve efficiencies as high as 75% [*49*].

An efficient hybrid must precisely balance both the energy and mass flow of the two systems. Thermal energy given off by the SOFC and chemical energy entrained in the anode off gas must meet turbine requirements. The mass flow of air driven by the turbine must maintain the thermal tolerances of the SOFC [*15*,*3*]. Pre-heating is often required to operate the cell stack efficiently otherwise degradation of the cell material can be expedited [*3*].

Many configurations of SOFC based hybrid systems have been investigated [*41*] [*3*,*4*] [*49*] [*1*,*3*,*4*,*37*,*41*,*49*]. Different configurations of FC-GT's depend mainly on the size of the system, power generation needed, and capital cost [*50*,*51*,*52*]. The arrangement of topping cycles (fuel cells placed before the turbine), bottoming cycles (cells placed after the turbine), or a combination of both have presented a library of challenges for those who wish to design and manufacture fuel cell gas turbine hybrids.

McLarty et al investigated the sub-optimal performance of integrating SOFC's with turbomachinery in a topping cycle configuration. Hybridization introduced mismatched dynamics, and off-design performance did not perform as expected. They found that the tightly coupled thermal and mass integration hinders dynamic response, as the large thermal mass of the fuel cell increases thermal inertia of the system, which then requires a larger surge margin in the turbomachinery, and limits the time-scale of response [*14*]. Noriko [*11*] also cited the start-up and turn-down times in topping cycle FC-GT's to be a challenge. SOFC's take significantly longer time to reach operational temperature and/or shut down compared to a gas turbine. Gas turbines, particularly 'peaker' plants are utilized in the energy market for their fast response to a dynamic electric load [*53*]. Thus, fast responding topping cycle FC-GT's require additional pre-heating for operation.

Traverso et al [*54*] attempted to model off-design turbine performance of a topping-cycle hybrid while assuming fixed fuel cell performance parameters. In their publication, the authors attempted to control the either the fuel flow rate to the turbine, or the electrical current of the fuel cell. The efficiency of the system was near 60% FTE at nominal turbine and fuel cell sizing. The authors noted, however, that this balance can only be achieved with appropriately sized equipment (i.e. fuel cell and turbine) and at precisely one operating condition, a result found by other authors as well [*55*]. The modeled hybrids were found to not be marketable for distributed electric markets or cogeneration plants due to poor part-load and off-design performance.

Song et al [*38*] attempted to scale a small (<kW) FC-GT topping cycle hybrid to a multi-MW class for large power generation. They incorporated off-design models of both the fuel cell and

the gas turbines in their modeling study. Their research relied on modeling a varying fuel flow rate to the fuel cell or gas turbine, or varying the incoming air to the GT system. It was found that simultaneous control of two of the three variables resulted in increased efficiencies from 35% to 58%. The configuration was limited by high temperature gradients across the SOFC however.

Operational prototypes [*56*] have achieved system integration through the introduction of multiple ancillary systems such as heat exchangers, combustors, and afterburners. These prototypes have found that introducing more components to the system without a way to control the parameters of the highly coupled system increased the risks of turbine failure and/or decreases in the overall efficiency of the system. The resulting analyses become gross over and/or under estimation of the design parameters and system performance.

3.2.1. FC-GT Economics

The market for FC-GT hybrids is limited by high capital cost [*52*] – specifically in the SOFC component. And continued problems in maintaining steady stack temperature while minimizing degradation of the components [*57*]. With high risk and higher cost of power generating fuel cells, the market for FC-GT's has yet to become novel. These problems have slowed development of FC-GT hybrids, and will continue to so long as novel system configurations and/or affordable components continue to evade us.

3.3. System Pressurization

It is well noted in literature that higher pressures increase the open circuit potential of a fuel cell. Winkler et al [*37*] proposed a topping cycle system where the fuel cell was taken out of the working fluid of the gas turbine through a series of pumps and blowers. The system was still

tightly coupled thermally and lacked sufficient controls to control the air flow directed to the SOFC. Parasitic compression for the fuel cell operation decreased efficiency and increased cost of the system as well.

The first tests of a pressurized FC-GT prototype were conducted at the University of California, Irvine in 2001 [*58*]. The hybrid system used a tubular fuel cell system producing 180 kW and was paired with a 75-kW Ingersoll-Rand turbine. The system could produce 220 kW over 2900 hours of testing at the National Fuel Cell Research Center. The fuel cell remained pressurized by being placed within the working fluid of the GT. Pressurization of the fuel cell stack within the turbine introduced the problem of balancing the thermal energy of the SOFC component. McLarty et al believed that control systems, such as bypass or recirculation, which partially de-couple the air flow rate between the turbine and fuel cell were necessary to expand the operating range with some trade-off in peak efficiency [*59*]. Others [*52*,*60*,*61*] have proposed alternative configurations for the FC-GT hybrids where internal reformation of natural gas provided the necessary thermal balance for the pressurized fuel cell. This proposal has shown promise if the reaction kinetics of steam reformation can be properly modeled and controlled within the pressurized cell stack.

Kuchonthara et al [*62*] investigated the effects of GT pressure ratios and turbine inlet temperatures on total FC-GT system efficiencies. Their modeled SOFC-GT incorporated both heat recovery and steam recovery to push the GT system of the hybrid to even higher efficiencies. They concluded that low TIT's required low pressure ratios to avoid excess fuel being consumed in the GT and allow for reasonable heat and/or steam to be recuperated. They also concluded

the corollary. High TIT's gained additional efficiency points at high pressure ratios due to a pressurized fuel cell and additional expansion power in the turbine. As such, this thesis will maintain high TIT's for dFC-GT modeling. Micro-turbine arrangements with low pressure ratios will be given a constant TIT as well, albeit lower than the original dFC-GT's TIT.

To summarize, literature and experimentation have unveiled common issues delaying the advancement of FC-GT's. These issues include:

1) The highly coupled nature of the hybrid system.
2) The mismatched dynamics during off-design operation, including increased surge/stall risk.
3) Thermal balancing of a pressurized SOFC system.
4) High capital investment.
5) Dynamic response of the system.

This steady-state study will aim to address issues 1-4 by de-coupling the FC-GT hybrid. In de-coupling the system, additional controls will be introduced to help account for mismatched dynamics. Pressurization of the fuel cell in this study will be accomplished with a small parasitic compressor, and thermal balance of the fuel cell will be accomplished through internal steam reformation. This study aims to also reduce the high capital costs of FC-GT hybrids by envisioning the proposed system as a retro-fit to existing GT systems. De-coupling the system could also allow the gas turbine to maintain transient capability and not hinder dynamic response, but that is beyond the scope of this study.

4. Component Models

This chapter will describe the complete model that utilizes first-principles to analyze the performance and designate a design space for the de-coupled FC-GT. It is assumed that internal steam reformation is capable of thermally balancing the fuel cell, and thermal gradients are not varying dynamically. Two engines are considered, a single-spool axial flow gas turbine and a smaller radial flow micro-turbine with exhaust regeneration. Both engines contain turbomachinery of a gas-turbine (compressor, turbine), a gas turbine combustor, SOFC, and OTM modules. The micro-turbine system includes a built-in heat exchanger to recover thermal energy from the turbine effluent. Advanced cycles with intercooling or heat recovery steam generators are not considered in this preliminary analysis.

4.1. Compressor/Turbine Model:

The primary compressor which is driven by the turbine compresses ambient air to the operating pressure of the turbine. A secondary compressor re-compresses the cooled oxygen permeate back to the operating pressure of the fuel cell. The isentropic efficiency definition for a compressor (29) is used in conjunction with an energy balance (30) and a property calculation (29,30) to estimate the compression work and outlet temperature of each compressor. The net power of the turbomachinery includes the efficiency of the turbine (27) as well. Efficiency of the compressor was based on specifications of common gas turbines, and NIST's tool REFPROP was utilized for property calculations

$$\eta_C = \frac{h_s - h_{in}}{h_{out} - h_{in}} \tag{29}$$

$$\dot{W} = \dot{m}(h_{in} - h_{out}) \tag{30}$$

$$T_s = T_{In} \cdot P_{ratio}^{1-\frac{1}{\gamma}} \quad (31)$$

$$h_s = h(P_{out}, s_{in}) \quad (32)$$

$$\eta_T = \frac{h_{In} - h_{out}}{h_{in} - h_s} \quad (33)$$

4.2. OTM MODEL:

OTM operation balances oxygen flux and degradation with typical operating temperatures near 800°C. Operating conditions for the OTM will vary slightly with specific material properties of the manufacturer, but generally accepted operating temperatures range from 700-900°C *[21, 22, 26-28]*. High compression ratios or exhaust heat recovery can raise the incoming air stream to these temperatures, but some pre-heating via a pre-combustor may be required between the OTM and compressor, determined by equation 28.

$$Q_{Preheat} = \dot{m}\left(h_{800°C} - h_{C,Out}\right) \quad (34)$$

The actual oxygen flux through an OTM is highly dependent upon the material properties, operating temperature, and oxygen partial pressures. To maintain generality this paper will consider oxygen separation as a percent of maximum theoretical recovery, R_T, defined as the limiting case where partial pressures in the permeate and non-permeate streams are balanced. Balancing these partial pressures results in (35) where X_{feed} is the inlet composition and P_{OTM} is the permeate pressure and P_{GT} is the turbomachinery operating pressure. The actual molar flux of oxygen separated from the compressed air stream is found by (36) where α is the ratio of actual recovery to theoretical recovery.

$$R_T = 1 - \frac{(1-X_{feed})*P_{OTM}}{X_{feed}(P_{in}-P_{OTM})} \quad (35)$$

$$\dot{n}_{O2} = \alpha R_T \cdot X_{feed} \cdot \frac{\dot{m}_{C,out}}{\mathcal{M}} \quad (36)$$

Lower permeate pressures correspond to higher recovery rates (R_T). Actual O_2 recovery is significantly less than R_T, and is dependent upon the area specific flux. Larger surface areas of OTM increases the net oxygen recovery with exponentially diminishing returns due to the lower driving force of partial pressure difference. In practice 75% of theoretical recovery showed the greatest potential for commercialization as an oxygen production system [*63*,*64*,*65*]. In a dFC-GT arrangement a significantly lower recovery rate may be practical.

4.3. Fuel Cell Model:

A nodal electrochemical model captures the energy and mass balance of the fuel cell. The nodal model allows for analysis of current density, electrochemical reactions, and voltages across a design length of a fuel cell. At a constant ASR, the current density distribution can be plotted along the length of the cell.

Given the operating conditions of the fuel cell several simplifications can be made. The first assumes an indirect internal reformer which allows for complete conversion of methane through steam reforming prior to the fuel stream reaching the anode flow channels. Thus, the net flow out of the fuel cell can be found with (37), where $\dot{n}_{CH_4}$ is the supply of natural gas. The water gas shift reaction, $CO + H_2O \rightarrow H_2 + CO_2$, is given an effectiveness, ε_{wgs}. And has an energy release of Δh^0_{wgs}. Assuming 100% oxygen utilization allows the number of cells, *N*, to be directly

correlated to the oxygen flux of the OTM and the average electrical current density, i_{avg}, as identified in (38).

$$\dot{n}_{out} = 3\dot{n}_{CH_4} \tag{37}$$

$$N = \frac{\dot{n}_{O_2} \cdot 4F}{i_{avg} \cdot w \cdot L} \tag{38}$$

The open circuit voltage, *E(x)*, is calculated from the temperature, pressure, and reactant concentrations of the anode and cathode as a function of position, *x,* in the anode flow direction (39). The operating pressure of the fuel cell is assumed to be at or slightly above the turbine inlet pressure, P_{GT}.

$$E(x) = \frac{-\Delta G_{rxn}}{2F} - \frac{RT}{F} \ln\left(\frac{X_{H_2O(x)}}{X_{H_2}(x) \cdot X_{O_2} \cdot \left(\frac{P_{GT}}{100kPa}\right)^{\frac{1}{2}}} \right) \tag{39}$$

The concentrations of the steam and hydrogen, X_{H_2O} and X_{H_2}, are calculated as a function of position, (40) and (41), with the oxygen concentration, X_{O_2}, equal to 1 across the entire cathode.

$$X_{H_2}(x) = 1 + \frac{\varepsilon_{WGS}}{3} - \frac{2\dot{n}_{O_2} \cdot r}{3\dot{n}_{CH_4}} - \frac{W(1-r)}{6F \cdot \dot{n}_{CH_4}} \int_0^x i(x)dx \tag{40}$$

$$X_{H_2O}(x) = \frac{2\dot{n}_{O_2} \cdot r}{3\dot{n}_{CH_4}} - \frac{1+\varepsilon_{WGS}}{3} + \frac{W(1-r)}{6F \cdot \dot{n}_{CH_4}} \int_0^x i(x)dx \tag{41}$$

The percent of anode exhaust recirculation necessary to achieve sufficient steam to carbon ratio, *S2C*, to avoid coking is represented by *r*.

$$S2C = \frac{r}{\dot{n}_{CH_4}} \cdot \left[\frac{2 \cdot \dot{n}_{O_2} - (1+\varepsilon_{WGS}) \cdot \dot{n}_{CH_4}}{(1-r)} \right] \tag{42}$$

The current distribution, *i(x)*, can then be solved iteratively using (43) subject to the average current density constraint of (44) and steam to carbon ratio constraint of (42). The area-specific-resistance, ASR, is assumed to be known and constant.

$$i(x) = \frac{E(x)-V}{ASR} \tag{41}$$

$$\int_0^L i(x)dx \cdot w = J = \dot{n}_{O_2} \cdot 4F \tag{42}$$

$$J = \dot{n}_{O_2} \cdot 4F \tag{43}$$

The fuel flow rate is calculated such that the stack achieves thermal equilibrium between the heat released in the electrochemical reactions, $\Delta h^0_{H_2}$, and the water-gas-shift, and the endothermic cooling of the steam methane reforming, Δh^0_{smr}. Equation 38 is solved such that ΔE = 0, in conjunction with equations 37 to 43. Hydrogen utilization within the stack is computed from the current and the potential H_2 supplied to the cell per equation 45. An energy balance can then be derived to solve for the flow of $\dot{n}_{CH_4}$ required to balance the system. The energy balance depends on the flow and specific enthalpies of the components entering the system, the flow and energy leaving the system, and the reactions occurring within the cell ($\dot{Q}_{Gen}$) as well as the reactions in the reformer ($\dot{Q}_{Reform}$).

$$\Delta E = \dot{Q}_{Gen} - \dot{Q}_{Reform} \tag{44}$$

$$\dot{Q}_{Gen} = \left(\frac{-\Delta h^0_{H_2}}{4F} - V\right) \cdot J \cdot N \tag{45}$$

$$\dot{Q}_{Reform} = \dot{n}_{CH_4} \cdot \left[\varepsilon_{WGS} \cdot \Delta h^0_{wgs} + \Delta h^0_{smr}\right] \tag{46}$$

$$Utilization = \frac{J \cdot N}{8F \cdot \dot{n}_{CH_4}} \tag{47}$$

The concentrations of carbon dioxide and carbon monoxide at the anode exit can be found using (48) and (49).

$$X_{CO_2}(L) = \frac{\varepsilon_{WGS}(1-r)}{3} \tag{48}$$

$$X_{CO}(L) = 1 - X_{CO_2}(L) - X_{H_2}(x) - X_{H_2O} \tag{49}$$

Total power and efficiency of the cell stack based on the power out, and the energy of the fuel supplied to the stack can finally be calculated as:

$$\dot{W}_{Fuel\ Cell} = V \cdot J \cdot N \tag{50}$$

$$\eta_{Fuel\ Cell} = \frac{\dot{W}_{Fuel\ Cell}}{\dot{n}_{CH_4} * LHV_{CH_4}} \tag{51}$$

4.4. Combustor Model

The pre-combustor raises the temperature of the compressed air to the operating temperature of the OTM, while the post-combustor raises the temperature further to that of the turbine inlet temperature. The working fluid of the turbine- oxygen depleted air – is heated by burning either natural gas or the anode exhaust products of the fuel cell. Turbine inlet temperatures are found solving the energy balance of (48) and reaction enthalpies: $\Delta h^0_{CH_4}$, Δh^0_{CO}, $\Delta h^0_{H_2}$, corresponding to the combustion of CH_4, CO, and H_2 respectively. Under some operating conditions the fuel cell exhaust contains insufficient chemical energy to raise the products to the desired turbine inlet temperature. Under these conditions, make-up fuel is provided. Under different conditions there is excess hydrogen in the anode exhaust which must be extracted prior to combustion to prevent overheating the turbine. Under the ideal scenario, the wasted fuel of the fuel cell provides precisely the energy desired by the turbine. A steady state analysis can determine the relative size of the two components that results in this complementary integration under different operating conditions i.e. current density, for the fuel cell.

$$\Delta E = \dot{n}_{air} h_{air} + \dot{n}_{Anode}\left(h_{Anode} + X_{CO}(L) \cdot \Delta h^0_{CO} + X_{H_2}(L) \cdot \Delta h^0_{H_2}\right) \tag{52}$$

In situations where the anode exhaust does not contain sufficient energy to power the turbomachinery, additional fuel balances the energy equation. The highly humidified combustor

fuel burned in the low oxygen residual air likely decreases pollutant formation considerably.

System Integration

Hybrid system performance was calculated by summing the outputs of the two generating components (equations 24, 46) and accounting for all heat addition steps. $Q_{PreHeat}$ is the name given to the variable that accounts for the pre-heating need of the OTM. This value increases the heat flow into the system and lowers the system efficiency, thus it is more beneficial to arrange the dFC-GT in such a way that pre-heating can be reduced and greater system efficiencies may be achieved.

$$\eta_{dFC-GT} = \frac{\dot{W}_T - \dot{W}_{C1} - \dot{W}_{C2} + \dot{W}_{Fuel\ Cell}}{(\dot{n}_{CH_4} + \dot{n}_{sup}) \cdot LHV_{Fuel}} \quad (53)$$

Equation 53 outlines the values governing the system performance of the dFC-GT. The total power of the hybrid system is calculated from the power produced by both the fuel cell and the gas turbine. The total power is reduced by a parasitic compressor needed to re-pressurized oxidant flow to the fuel cell (see Figure 9). The energy of fuel input to the system is calculated using lower heating values of the chemical components within the fuel. Combustor fuel is assumed to be pure natural gas (CH_4) while the anode fuel is combination of hydrogen (H_2), carbon monoxide/dioxide (CO, CO_2), and water (H_2O). The LHV of each chemical component present in the system is outlined in Table 2Table 1.

Table 1 Lower Heating Values of Chemical Components

Molecule	Lower Heating Value (LHV)	Unit
CH_4	802,301.00	kJ/kmol
CO	283,004.70	kJ/kmol
CO_2	0.00	-
H_2	241,826.40	kJ/kmol
H_2O	0.00	-
O_2	0.00	-
N_2	0.00	-

5. Steady State Analysis

The primary thermodynamic difference between dFC-GT and other hybrid configurations is that the dFC-GT recovers all the fuel cell waste heat as hydrogen which is then converted to heat at higher temperature in the combustor. This arrangement thus enables intermediate and low temperature SOFC technology to achieve the same thermal integration originally envisioned for SOFC operating more than 1000°C. The primary mechanical difference is the removal of the SOFC from the turbine working fluid, maintaining turbine stability during transient operation. Pressurization of the SOFC improves performance and allows for direct use of the exhaust without re-pressurization prior to the combustor. Figure 11 presents a high-level visualization of the dFC-GT energy balance as a series of black boxes, represented by equations 54-56.

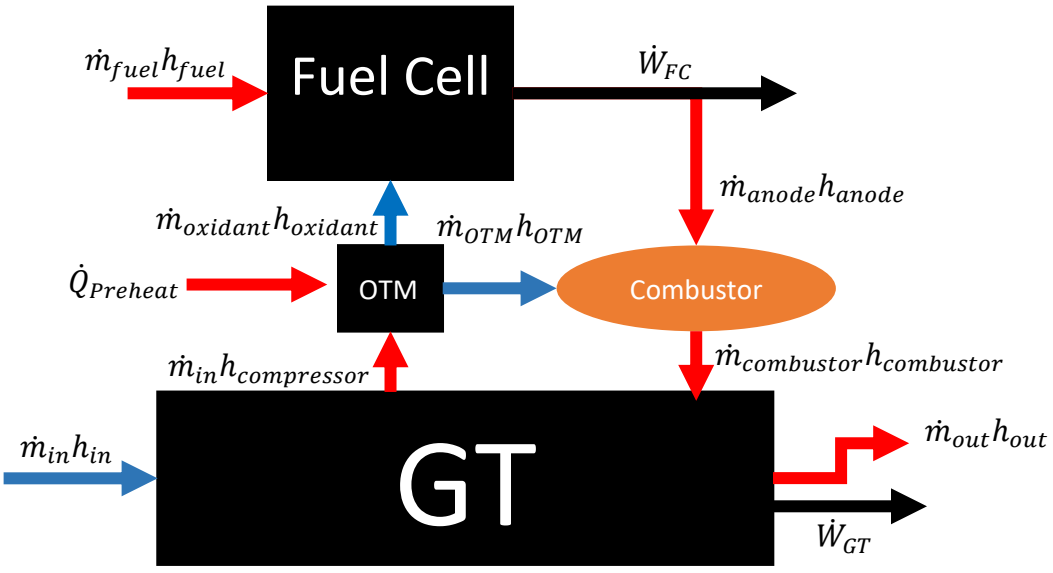

Figure 11 Black box diagram of dFC-GT

For the gas turbine/OTM:

$$\dot{m}_{in}h_{in} + \dot{m}_{anode}h_{anode} + \dot{Q}_{Preheat} = \dot{m}_{oxidant}h_{oxidant} + \dot{m}_{out}h_{out} + \dot{W}_{GT} \quad (54)$$

Where $\dot{m}_{anode}h_{anode}$ and $\dot{m}_{oxidant}h_{oxidant}$ connect to the fuel cell:

$$\dot{m}_{oxidant}h_{oxidant} + \dot{m}_{fuel}h_{fuel} = \dot{m}_{anode}h_{anode} + \dot{W}_{FC} \quad (55)$$

The total system energy and mass balance then becomes:

$$\dot{m}_{in}h_{in} + \dot{m}_{fuel}h_{fuel} + \dot{Q}_{Preheat} = \dot{m}_{out}h_{out} + \dot{W}_{FC} + \dot{W}_{GT} \quad (56)$$

5.1. Design Space Investigation

To investigate the system performance of the dFC-GT a design space was conceptualized based on previous hybrid models, commercial turbomachinery, and current SOFC technology. Determining the design point for the dFC-GT system required assumptions of specific operating conditions. Literature *[56]* states standard fuel cell current densities to be .5 A/cm^2, with a standard area specific resistance (ASR) of 0.25Ωcm^2. The steam to carbon ratio (S2C) of 2.00 was chosen to allow for sufficient humidification to avoid coking and promote water-gas shift reactions (WGS).

Using these values as the basis for the design space investigation; the operating voltage of the fuel cell can be determined using the nodal fuel cell model energy balance (equations 44-47). Solving the energy balance at this current density provides a fuel cell operating voltage of .936V. At this high of an operating voltage, less endothermic steam reformation is required and

thus the fuel utilization in the fuel cell increases, up to 74%. The remaining 26% of hydrogen available in the fuel cell is sent to the combustor of the gas turbine. At this percentage of hydrogen exhaust, a 22MW fuel cell can drive a 5MW gas turbine with no additional fuel required in the combustor.

Modeling the system at this current density conditions yielded a combined system efficiency of 75.4%; a SOFC efficiency of 66.1% and a gas turbine efficiency of 35.4%. Parameters were varied from initial conditions to model an overall design space shown in Figure 11. Sensitivity of each varied parameter was investigated and shown in Figure 13. Additional design point values and their respective modeling ranges are presented in Table 2.

Table 2 Nominal Design Parameters

Design Variable	Value	Typical Ranges	Units
Current Density	.5	.105-1.5	A/cm^2
ASR	.25	.25-1.25	Ωcm^2
Steam to Carbon Ratio	2	-	~
Turbine PR	15	5-15	~
Permeate Pressure	50	50-250	kPa
Mass Flow	20	4-100	kg/s
Turbine Inlet Temp	1200	1100-1300	K
η_C	80	75-85	%
η_T	88	82-92	%

Commercial turbomachinery can be purchased with power outputs ranging from 30kW to 520MW (GE 9H) operating with pressure ratios from 3:1 up to 24:1 (Titan 250). The study presented assumes a pressure ratio of 15:1 for power generation with a mass flow inlet of 20 kg/s, typical for engines in the 10-25 MW range. Smaller engines (<500kW) with pressures

suitable for oxygen recovery, i.e. >10:1, are still under development. Operation at 1MPa or higher is desirable to limit the vacuum which must be drawn on the permeate side of the OTM.

Table 3 Nominal dFC-GT Performance

	Nominal Value	Operating Range	Unit
SOFC Voltage	0.936V	0.77-0.97	Volts
Hydrogen Utilization	74.0%	48.8-83.1	%
Anode Recirculation	59.6%	85.1-53.6	%
Oxygen Recovered	49.7% of R_T	16.5-82.5	%
dFC-GT Efficiency	75.4%	55.0-82.1	%

Nominal operating conditions assume *1)* Combustion of the anode-off products with the depleted air raises the pressurized air's temperature to the nominal turbine inlet temperature (TIT), and *2)* the fuel cell utilizes all recovered oxygen from OTM in the electrochemical reactions, resulting in oxidant flow directly correlated to the net current. Table 3 details the calculated utilization and recirculation of the fuel cell, recovery of the OTM, and efficiency of the system.

The performance of a SOFC is primarily defined by its operating voltage, current density, and hydrogen utilization. Current density and voltage have an inverse relationship as defined by equation 41. Since the dFC-GT is constrained to thermally balanced operation the hydrogen utilization and voltage are linked through the energy balance of equation 44. Anode recirculation is calculated through the design S2C and equation 38. Oxygen recovery is defined as percent of theoretical and calculated through the design permeate pressure and equation 35.

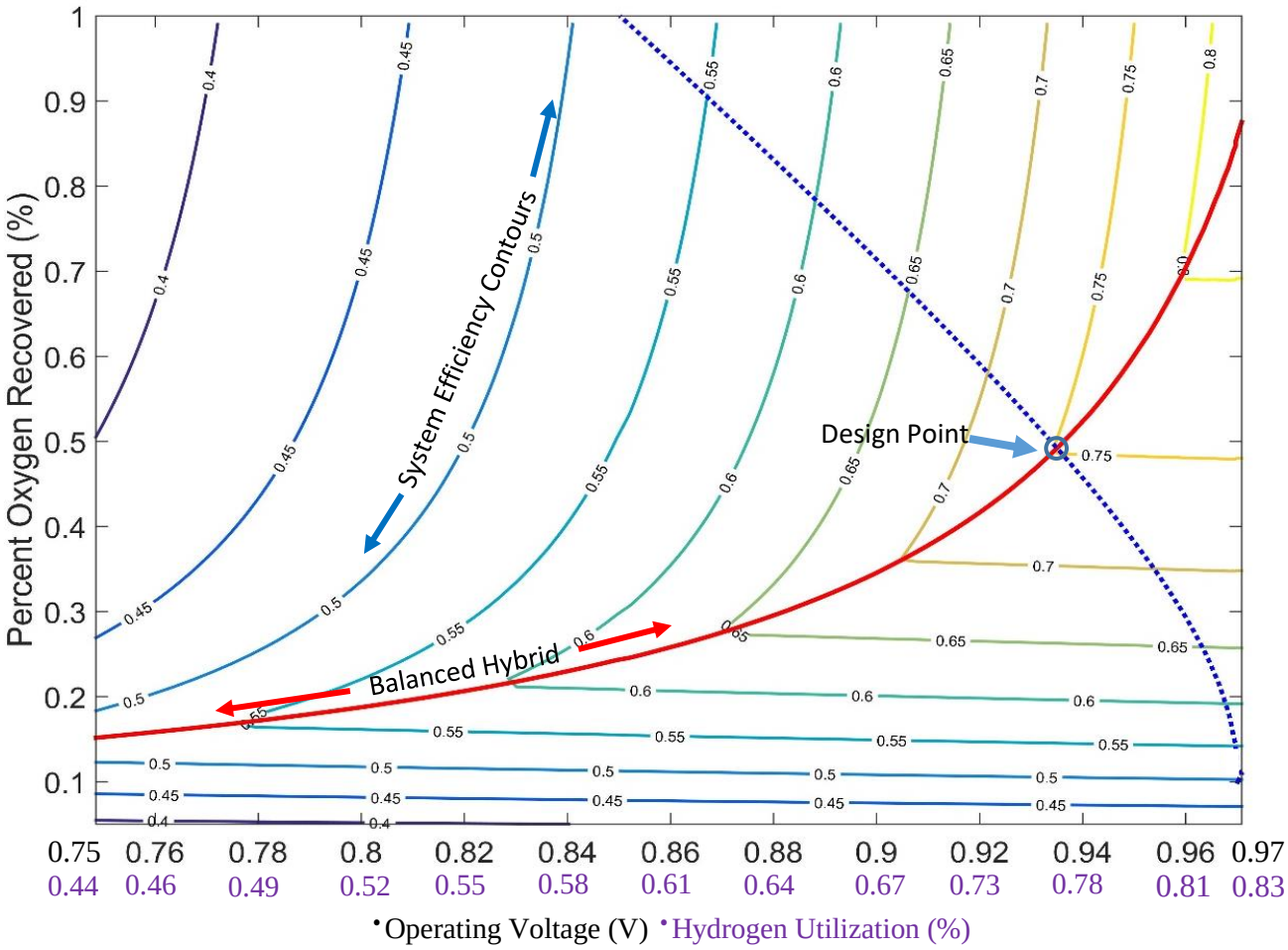

Figure 12 Characteristic Curve of dFC-GT System

Figure 12 illustrates the design space generated for a dFC-GT operating at 1.5 MPa. The operating voltage varies from 0.75V to 0.97V along the *x*-axis. The increase in voltage correlates to a more efficient fuel cell system, thus the heat generation decreases, and the fuel utilization increases from 44% to 83%. The percent of theoretical oxygen recovery along the y-axis generates a larger fuel cell system in the model to utilize all incoming oxidant. The overlaying contours denote the total system efficiency achievable in the model. The design point is at .936V and 49.7% oxygen recovery. To understand this plot further, it is worthwhile to break it down into its components.

Figures 12 and 13 hold the compressor inlet flow rate, the turbomachinery efficiencies, and OTM back pressure constant, while showing the "operating line" of the dFC-GT. The solid line shown indicates a thermally balanced hybrid, where combustion of the anode exhaust products results in the nominal turbine inlet temperature of 1200K. This line demonstrates that a less efficient (lower voltage), smaller (lower oxygen recovery) fuel cell can power the same turbomachinery as a larger, more efficient fuel cell system. The increased hydrogen utilization at elevated voltage reduces the combustible energy of the anode exhaust. Therefore, a larger SOFC is needed to sustain the turbomachinery as indicated by the upward trajectory of the dark solid line. Lower voltages correspond to smaller SOFC systems paired to the same gas turbine, requiring less oxygen and a smaller OTM.

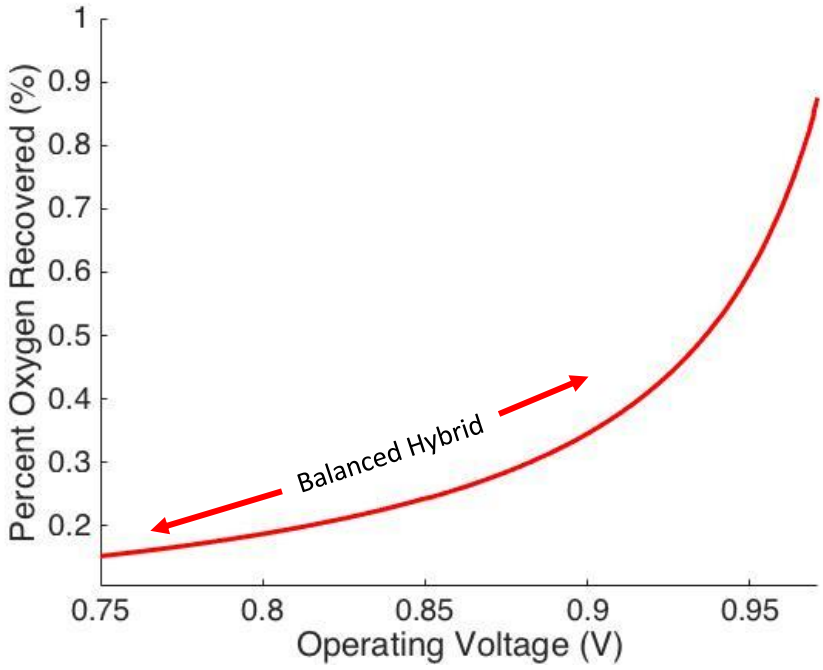

Figure 13 Operating line of dFC-GT

The solid red line demarks the boundary between two important regions. Below the line corresponds to an undersized fuel cell which does not produce enough waste energy (i.e. hydrogen) to drive the turbine at optimal conditions. Less oxygen recovery is necessary, but additional fuel must be combusted to reach the nominal turbine inlet temperature. In this area a greater portion of the power is derived from the less efficient turbine, thus lowering the net efficiency of the hybrid. Above the solid red line represents an oversized fuel cell, the exhaust of which contains excess combustible energy which must be rejected to avoid overpowering the turbine. The unused anode exhaust products diminish the system efficiency in this region.

With the assumed ASR of 0.25 $\Omega \cdot cm^2$, the current density corresponding to the voltage range shown in the previous figures decreases from 1.5 A/cm^2 to 0.105 A/cm^2, assuming there are negligible heat losses and a 60% conversion of CO to CO_2. Table 4 gives details of average current densities as well as their associated operating voltages and hydrogen utilization.

Table 4 Voltage and Utilization of Average Current Densities (Figure 12)

Average Current Density (A/cm^2)	Operating Voltage (V)	Hydrogen Utilization (%)
1.50	.77	.488
1.37	.791	.510
1.23	.815	.536
1.09	.840	.568
0.950	.863	.603
0.810	.887	.642
0.669	.910	.685
0.528	.936	.731
0.387	.951	.777
0.246	.965	.815
.105	.973	.831

By constraining the dFC-GT model by the energy balance in equation 44 the current density of the fuel cell becomes intrinsically linked to the fuel utilization within the stack. This is

demonstrated in Table 4, showing that as you move to a more efficient fuel cell, i.e. higher operating voltage, less internal steam reformation is needed for cooling, and thus less fuel needs to be input to

In this study, the net current, and thus the size of the SOFC, scales with the percent oxygen recovered on the y-axis of Figure 12. The power output of the SOFC scales linearly with both the oxygen recovery and the operating voltage. Thus, the ratio of power output between the SOFC and the GT increases along the solid red line from 2:1 at a voltage of 0.80V, to 5:1 at the design voltage of 0.93V, and to 8:1 at 0.96V. Figure 12 demonstrates that higher system efficiencies are achieved by raising the fuel cell voltage and producing a greater portion of the power in the fuel cell.

The design voltage of 0.936V is significantly higher than most existing systems. The majority of this difference is due to the pressurization, a pure oxygen cathode, and lowered hydrogen utilization. An SOFC with the same ASR operating at an equivalent current density, typical atmospheric air conditions, and hydrogen utilization of 80% would produce a voltage of 0.83 V. This voltage would correspond to the operating conditions of most commercial SOFC manufacturers.

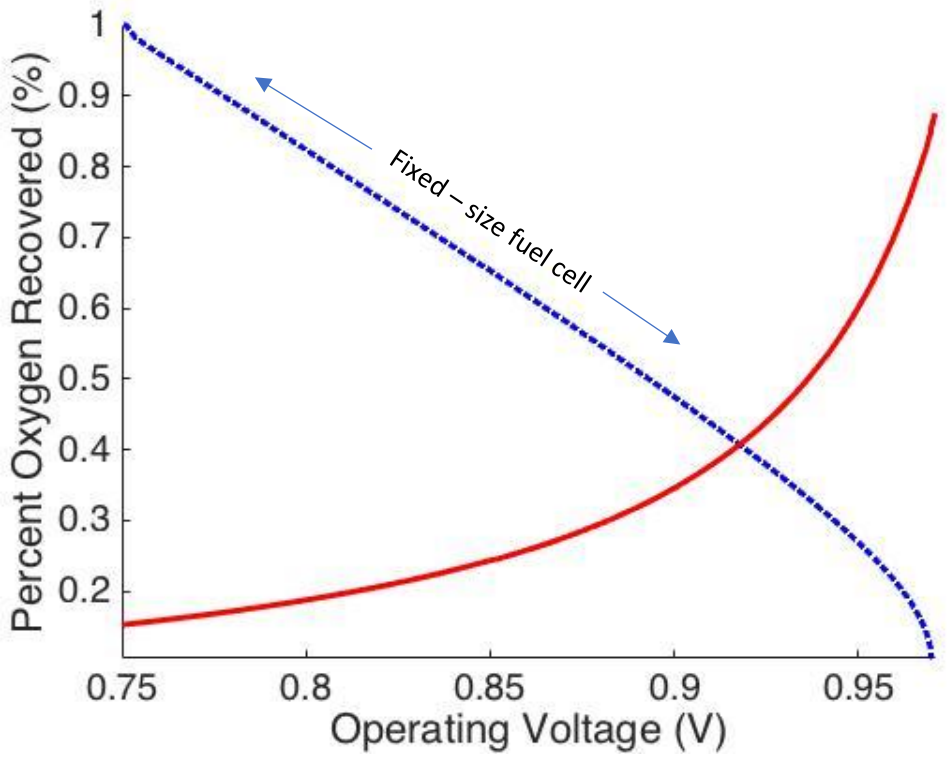

Figure 14 Fixed fuel cell size operating line

Figure 14 shows a the dotted line apparent in the middle of Figure 12 and indicates an operating line for a fixed size SOFC with varying oxidant supplied to its cathode. This line demonstrates the operating characteristics one would have if current densities of the fuel cell change according to the V-I relationship of a cell. This line illustrates the off-design (i.e. not balanced) performance of the hybrid system. Referencing back to Figure 12 it is apparent that achieving greater than 75% FTE efficiency becomes a small operating envelope near the nominal operating conditions, though efficiency remains above 60% for the majority of the operating range, a significant improvement over existing combined-cycle gas turbines or fuel cell gas turbine hybrids

At part-load, the relative power outputs may change considerably as the FC becomes more efficient and the turbine less. Achieving optimal integration over a range of outputs requires adjusting the turbine flow rate through changes in speed or inlet guide vanes, possibly firing the turbine with supplemental fuel, or extracting excess hydrogen from the anode exhaust prior to the combustor. Unlike the standard FC-GT topping cycle, the air flow rate is not linked to the temperature gradient in the SOFC, allowing for greater flexibility in the operation of the two sub-systems.

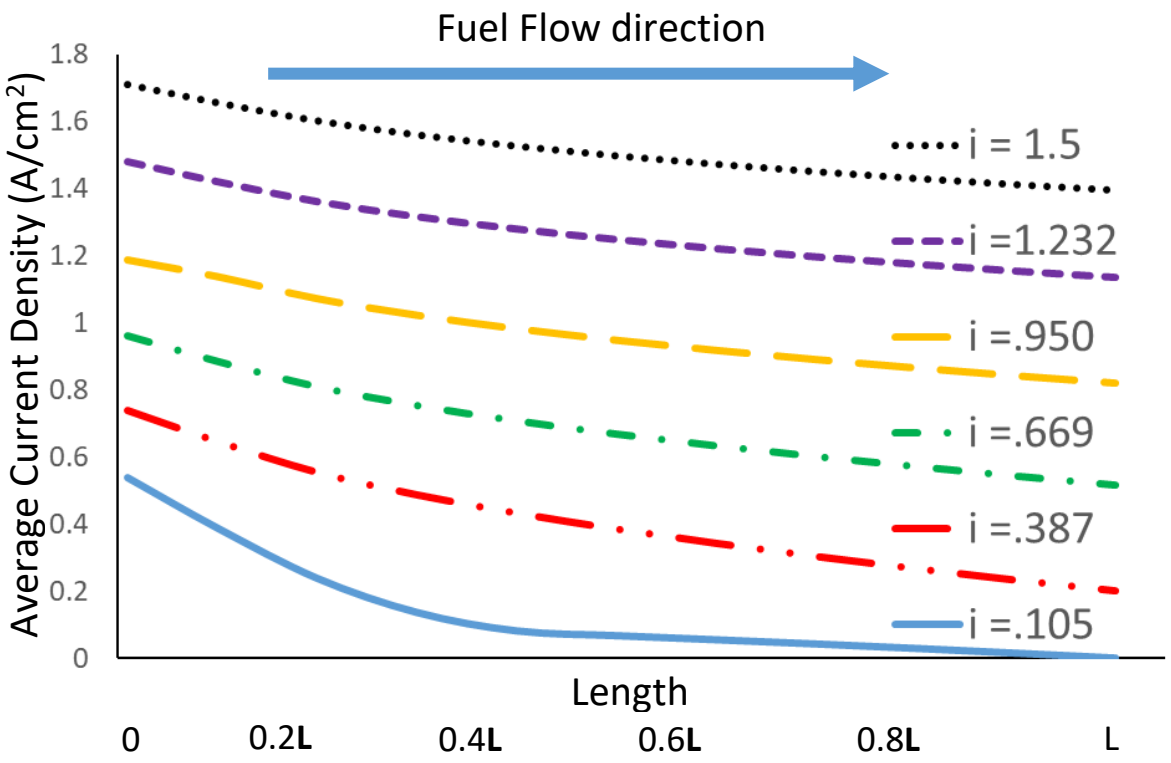

Figure 15 Current density distribution in a spatially resolved fuel cell model

The upper limit of 0.97V was not chosen arbitrarily. As the hydrogen utilization increases at high voltages, the hydrogen concentration at the end of the anode channel is reduced. Eventually the hydrogen concentration is low enough that the local Nernst potential is equal to the operating voltage, and the local current drops to zero. This is illustrated in Figure 15, which shows the current density profile along the centerline of the cell at different operating conditions and the local current density at the end of the anode channel. At the design pressure of 1.5MPa, the critical voltage when this occurs is 0.97V (the bottom-most line of Figure 15), corresponding to a hydrogen utilization of 83.1%. Higher voltage operation is not possible, unless utilization is reduced and some pre-reforming of the fuel is accomplished.

5.2. Sensitivity Study

To investigate the governing variables in the dFC-GT model, a sensitivity analysis can be conducted. This study showed which variables influenced the steady state model the most and is shown in Figure 14. It was found that the three most important factors in the current model were the fuel cell current density within the stack (illustrated in Figure 11), the back pressure controlling the oxidant flow exiting the OTM, and the pressure ratio of turbomachinery. OTM back pressure controlled the oxidant flow to the OTM, as well as determined how much re-pressurization was needed before being sent to the SOFC. The pressure ratio of the gas turbine affects both the gas turbine performance as well as the fuel cell open circuit voltage.

Current density was varied between 0.105 A/cm^2 and 1.50 A/cm^2. At constant ASR, this corresponded to the voltage range of 0.77V to 0.970V at 1.5MPa shown in Figure 11. At higher voltages, the dFC-GT achieves a fuel-to-electric efficiency of 82.6% by reducing the heat

generated in the fuel cell and thus requiring less fuel for endothermic reformation. Low voltage operation is then the corollary, increasing the heat generated by the fuel cell and thus requiring additional steam reformation is needed to thermally balance the system. This is achieved with additional excess fuel, lowering the overall efficiency of the system to 55%.

The total current is linked to the oxidant flow rate of the OTM by equation 38. This flow rate can be adjusted by either a) adjusting the OTM back pressure, or b) changing the OTM module surface area. This sensitivity analysis maintained constant oxygen flux, thus a decrease in the OTM back pressure corresponds to a significant decrease in the OTM surface area. The result is an increase in the parasitic compression work and decrease in available oxidant to the fuel cell, lowering the overall system efficiency.

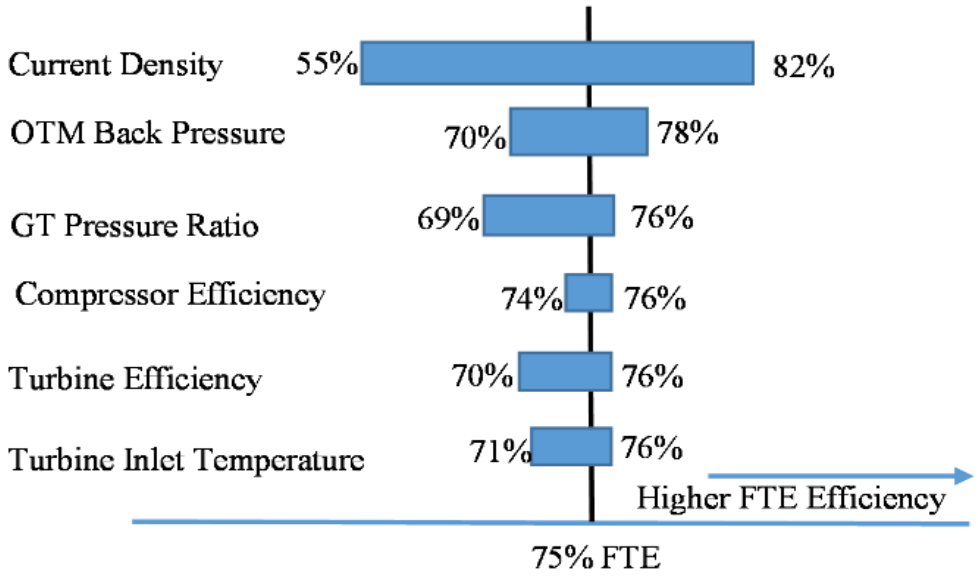

Figure 16 Sensitivity Study of dFC-GT System

The operating pressure and isentropic efficiencies of the turbine equipment both have a significant impact on overall performance as the turbine produces 20% of the system power. Similarly, the turbine inlet temperature has a significant impact on the overall efficiency. Higher

turbine temperatures imply that a greater portion of the power is produced from the turbomachinery. Since this power relies on combustion, it is less efficient than producing the power in the fuel cell. Relying on the fuel cell to generate more power in the systems improves the overall efficiency. This is beneficial, as achieving ideal turbine inlet temperatures at off-design conditions may prove difficult.

5.3. Fuel Cell and OTM Relationship

Assuming the SOFC and turbine are perfectly sized for each other, and that 100% of the recovered oxygen is utilized within the SOFC, then the recovery coefficient becomes directly linked to the design current density. A lower design current density raises the efficiency by operating at higher voltages, but at the cost of requiring additional SOFC active area. The trend illustrated in Figure 14 is a nearly linear relationship between system efficiency and the SOFC active area relative to the nominal design condition. Net efficiency rises from 62.0% to 78.0% as the active area is increased 200%. This corresponds to a current density reduction from .250 to 1.00 $A \cdot cm^{-2}$.

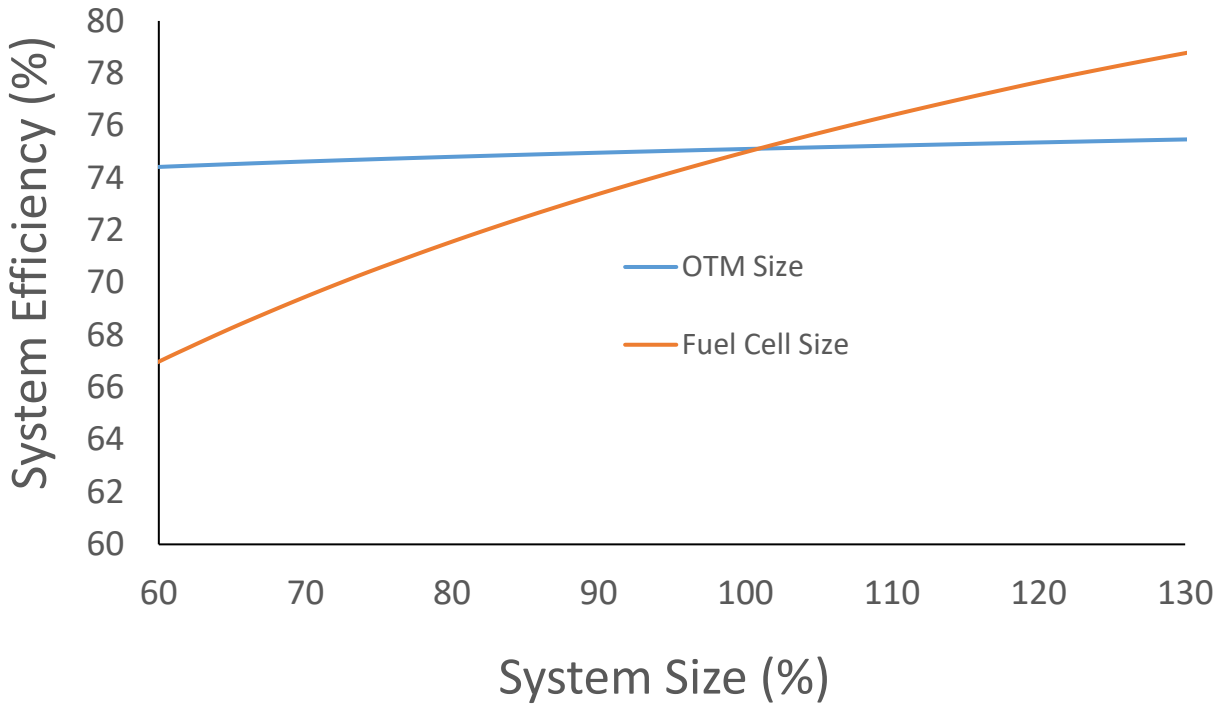

Figure 17 Relative Size of Fuel Cell and OTM Components to System Efficiency

Figure 18 shows that a similar range of OTM surface area has a much smaller impact on efficiency. Increasing the surface area within the OTM module corresponds to increasing the permeate pressure, thus lowering the parasitic load of re-compression at the expense of additional capital cost for the larger OTM module. The performance impact of increasing the permeate pressure is a net efficiency gain from 72.0% to 73.0% as the active membrane area is increased 200%.

5.4. System Pressurization

The operating pressure of the system affects efficiency through both the gas turbine and the open-circuit-voltage of the fuel cell. Net system efficiency, shown in Figure 19, increases from 68% to 73% as the system pressure is increased from 0.5Mpa to 2.5MPa with diminishing returns

beyond 1.5MPa. Heat recovery with a recuperated engine enables higher efficiency at lower operating pressure and will be discussed in later sections.

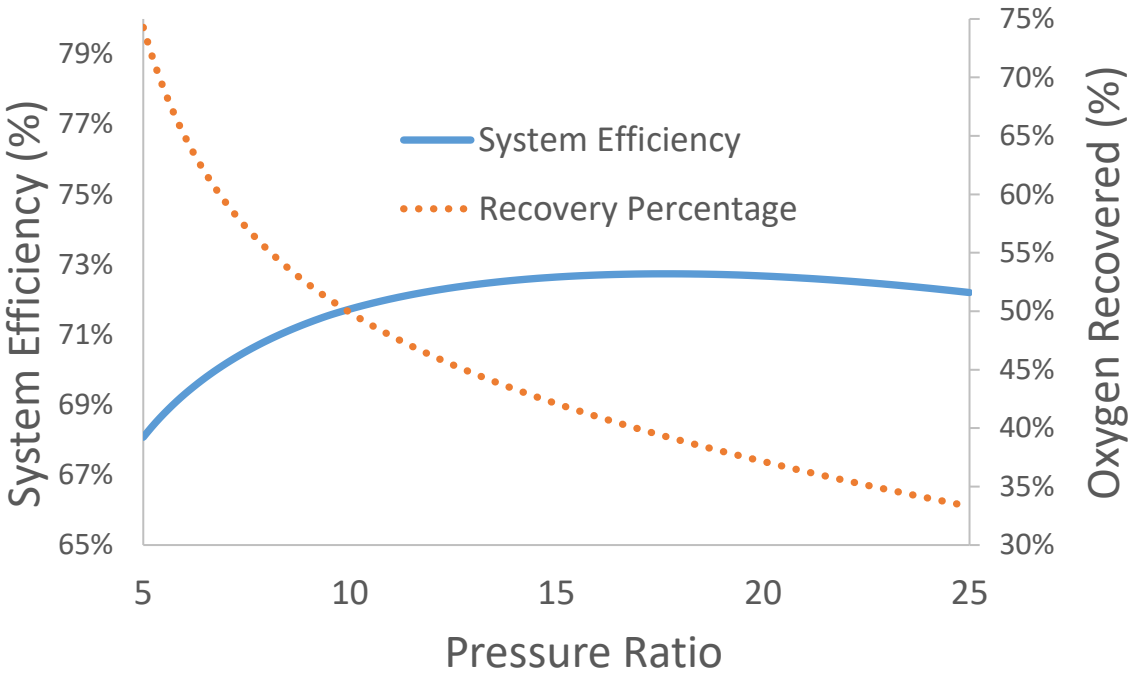

Figure 18 Pressure Ratio of GT vs Total System Efficiency and % Oxygen Recovered

Lower system pressures increase the heating required to achieve the same inlet temperature, thus requiring a larger fuel cell to drive the same mass flow through the lower efficiency turbine. Lower operating pressure also reduces the fuel cell voltage and limits the theoretical oxygen recovery in the OTM. Figure 19 illustrates how these impacts combine to lower efficiency and increase the percent of theoretical oxygen recovery that would be required at a current density of $0.5 A \cdot cm^{-2}$, assuming a permeate pressure of 50kPa. The high oxygen recovery at low operating pressure may be impractical, as the surface area of the oxygen membrane increases exponentially as it approaches the theoretical recovery limit.

5.5. Micro-turbines

Large SOFC (>20 MW) units are currently not in production and thus it is beneficial to examine the opportunities the dFC-GT presents for smaller sub MW systems. A smaller SOFC system could pair well with current micro-turbines produced today. Micro-Turbines typically operate at pressures between 300kPa and 500kPa and pressure ratios <5:1. At these low-pressure ratios the OTM preheating would increase significantly and the system efficiency would decline, as per Figure 19.

At lower pressure ratios, however, the outlet temperature of the turbine air is considerably higher than the air out of the compressor, enabling some heat recovery to be implemented to reduce, or even replace, pre-heating of the OTM. Table 5 shows the relationship of exit temperature versus compressor outlet temp.

By utilizing a heat exchanger that links the outlet turbine air to the outlet compressor air, pre-heating can be accomplished so much so that the pre-combustor of the dFC-GT can be removed. Figure 20 illustrates a schematic of the dFC-GT with the addition of exhaust heat recovery to pre-heat the compressed air to the 800°C. The recuperated cycle with a pressure ratio of 5:1, and mass flow of 6 kg/s can achieve a net fuel-to-electric efficiency of 77%. With an OTM pressure ratio of 25:1, the operating current density is limited to be above $0.4\frac{A}{cm^2}$ to allow for a reasonable oxygen recovery.

Table 5 Outlet Temps of Compressor and Turbine at Varying GT Pressure Ratio

GT Pressure Ratio	Compressor Outlet Temp (K)	Turbine Outlet Temp (K)
1:15	720.69	694.81
1:12	674.96	727.27
1:9	619.08	771.06
1:6	546.15	837.32
1:3	437.01	955.02

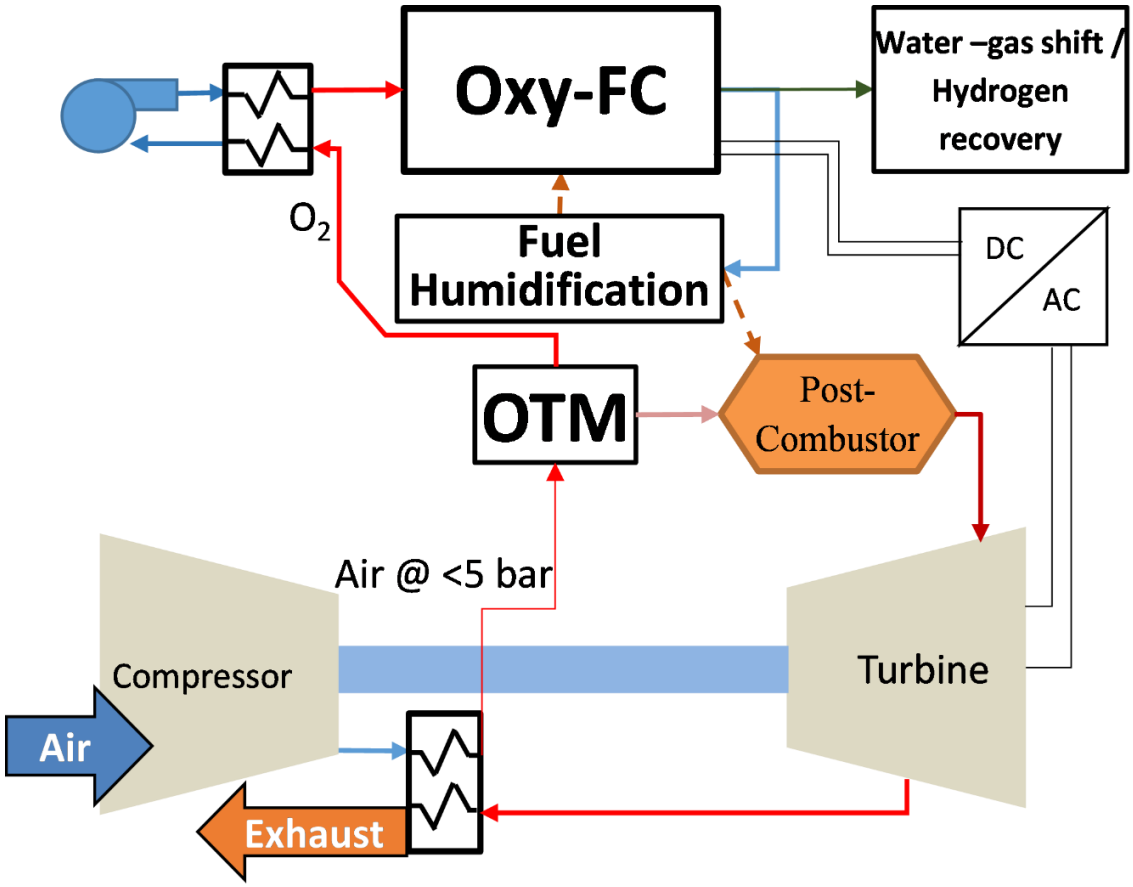

Figure 19 Schematic Drawing of de-coupled Hybrid with Heat Recuperation

Removing the pre-combustor and allowing OTM preheating to be accomplished by turbine waste heat significantly improves operating efficiency. The lower gas turbine size means lower

turbine inlet temperature would be necessary in the design. This enables more power generation in the fuel cell improving FTE even further. As the pressure ratio approaches 3:1 the back pressure of the OTM must be lowered further than 25:1 to allow for ample oxidant recovery. This would decrease system efficiency as the re-pressurization load increased.

The de-coupled nature of the dFC-GT would also benefit micro-turbines. Stable power generation via combustion in the gas turbine can be achieved during start up sequences; preheating of the OTM and SOFC would take place during this start up sequence. Once ideal temperatures have been met, control of the OTM permeate flow would be engaged, decoupling the system and allowing anode exhaust to continue powering the gas turbine. The micro-turbine configuration of the dFC-GT could provide a new CHP system for distributed generation systems and micro-grids, helping to reduce reliance on grid power.

5.6. Hydrogen Co-Production

A final benefit of the dFC-GT (in both large-scale and micro-scale) is the possibility for hydrogen co-production. Investigation of the hydrogen recovery technologies available is beyond the scope of this study, but some simple estimations can be made. Low hydrogen utilization in the SOFC provides a large hydrogen concentration in the anode exhaust, up to >50% at low operating voltages. The high hydrogen content is sufficient to power large-scale gas turbine engines as shown in the previous sections. Alternatively, the anode exhaust could be captured, filtered, and hydrogen byproduct could be obtained instead of supplying the mixing chamber of a gas turbine. In envisioning the dFC-GT as a retro-fit technology, specifically for ‘peaker’ plants, this hydrogen capture could be accomplished during non-peak hours. Then, when load demand

spikes, the hydrogen capture would end and the anode exhaust would be redirected to the combustor of the gas turbine.

Table 6 Anode exhaust H2 content at varying voltage

SOFC Operating Voltage (Volts)	SOFC Exhaust H_2 Concentration (%)
0.972	9.10
0.951	16.4
0.910	28.7
0.863	39.7
0.815	48.4
0.770	55.0

Table 6 shows the SOFC's exhaust hydrogen concentration at varying operating voltage. At the dFC-GT's nominal design condition (.936V) the anode exhaust hydrogen concentration is 21.3%. Several membrane and adsorption technologies are available that can capture a

significant portion of this hydrogen with minimal parasitic losses ([*12*]). Operation at 0.77V for the same sized fuel cell produces a 55.0% concentration of hydrogen in the anode exhaust.

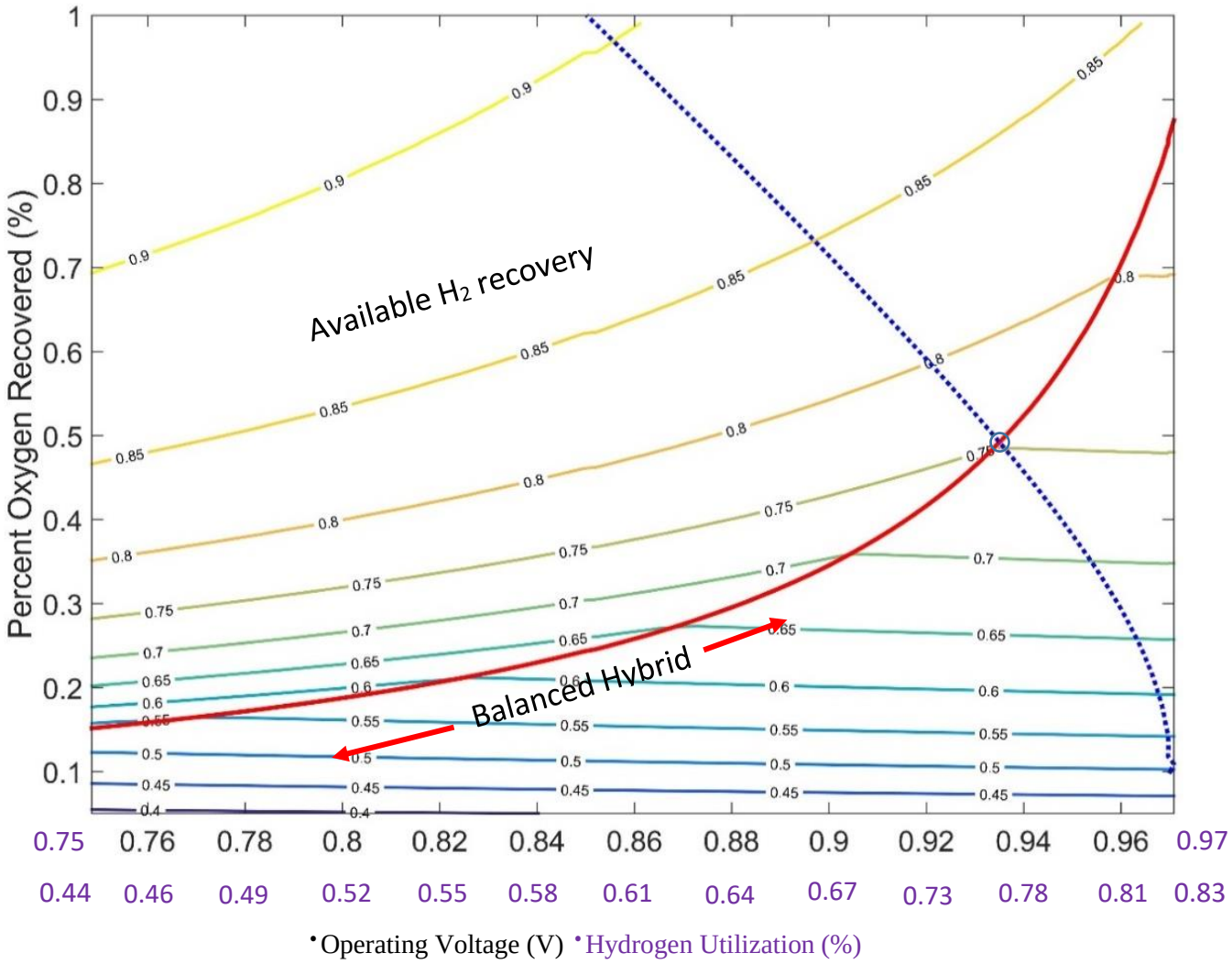

Figure 20 Characteristic curve of dFC-GT w/ H2 recovery

Figure 21 illustrates the additional energy recovery possible through hydrogen capture. The same regions, operating line, and design point all exist within Figure 21 as Figure 12. Fuel must be input below the solid operating line to reach a thermally balanced dFC-GT system. Above the operating line, however, no longer exists a region where a larger SOFC system

exhaust contains excess energy which must be rejected. Instead, hydrogen gas can be pulled off from the excess energy of the fuel cell exhaust and stored, raising the overall system efficiency. This allows the dFC-GT to work as both a fuel source and an energy production device.

Figure 22 provides additional detail around the design point of Figure 12. The original efficiency contours remain, with dotted overlaying contours showing the additional co-production efficiency if hydrogen recovery is considered. The dotted line passing from the upper left to lower right represents a fixed-size system operating at different power outputs. A lower voltage corresponds to a higher current, i.e. greater oxygen use, and an increase in net power output. The lower voltage increases the heat production, requiring additional fuel to maintain the temperature. The excess heat generation is captured in the form of extra hydrogen in the anode exhaust. 100% of this additional hydrogen is recoverable, since the unrecoverable hydrogen will still be used to drive the turbine. The additional energy recoverable as hydrogen exceeds the reduction in SOFC efficiency. Thus, as the FTE efficiency drops from 75% to 65%, the co-production efficiency would rise to 83% at a voltage of 0.90V.

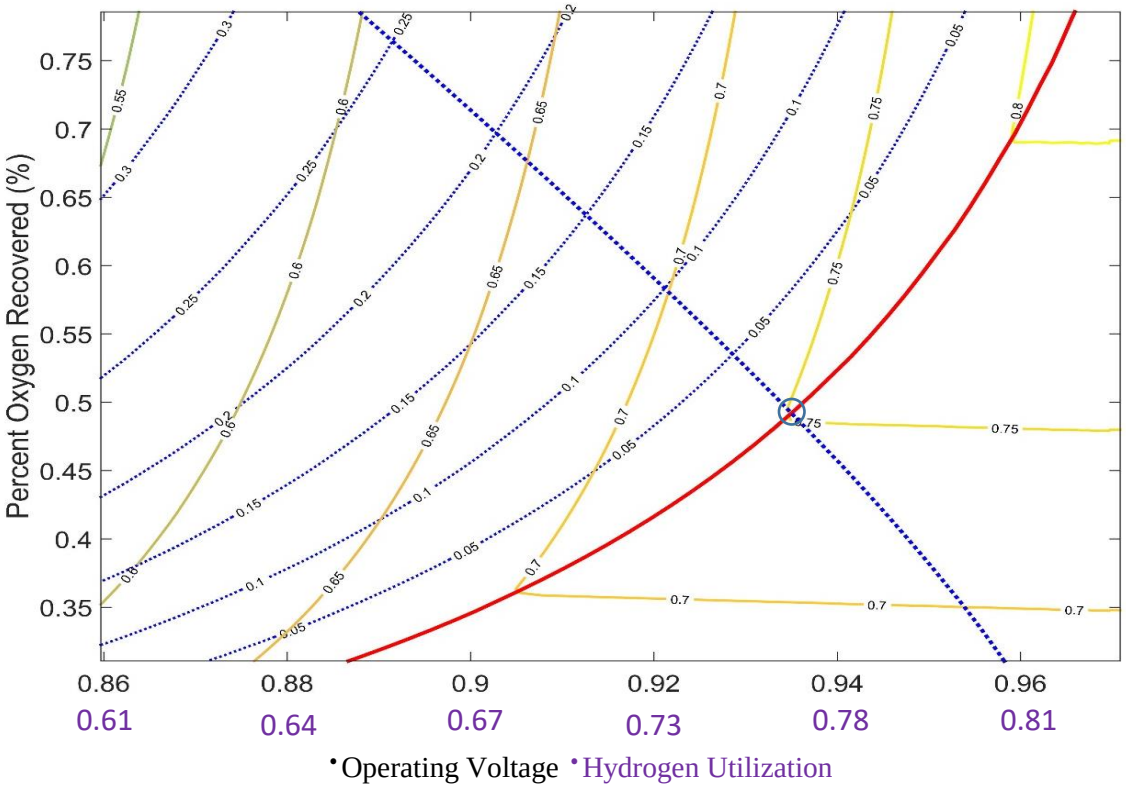

Figure 21 Detail of characteristic curve w/ hydrogen recovery at design point

A lateral translation where voltage drops with the current remaining fixed is representative of how the dFC-GT performs as the fuel cell degrades over time. The response to degradation is either *a*) a small increase in current to maintain nominal power, or *b*) a corresponding decrease in current to maintain operation on the solid red line representing the balanced operating condition. Option (*a*) further lowers the voltage, and thus the FTE efficiency, increasing the heat generation vented or recovered in the form of hydrogen. If the ASR were to degrade to 0.375Ωcm^2, a 50% increase, voltage would decrease to 0.83 and the current would increase 13% to maintain the same power output. This would lower FTE efficiency to 57%, but allow for co-production efficiencies up to 85%.

Option (*b*) avoids the challenge of capturing excess H_2, and maintains the highest FTE efficiency possible, but the simultaneous reduction in voltage and current significantly decreases the power output of the hybrid. For the same rise in ASR, thermally balanced operation would be achieved with a 20% reduction in current. At these conditions, the voltage would be 0.915V and the FTE efficiency would still be an impressive 71%, but the power output would have dropped by 22%.

Parasitic compression of hydrogen for storage would introduce another cost to the system. Compression of the hydrogen may use 2.2 to 3.3 kWh of energy to compress each kilogram. This corresponds to about 15-20% of the hydrogen energy recovered. At the current value of hydrogen, $3/kg [*66*], this represents a 10x increase in value using 3kWh of electricity valued at 0.1$/kWh to recover $3 of fuel. Thus, co-production of hydrogen can lead to continued profits through storage and resale of hydrogen gas.

6. Economic Analysis

This chapter presents a brief analysis of the cost and emissions trade-offs for a dFC-GT hybrid. The economics of electricity generation plants are immensely complex with continuous participation in evolving energy markets that seek to balance the ever-shifting demand and supply of electricity. Precisely forecasting the value of generated electricity over the 20 to 30-year lifespan of a power plant is impossible, thus broad assumptions will be made to compare a dFC-GT to its existing alternatives. The pricing trends in the electric sector continue to favor both responsive and energy efficient generation technologies, though few systems would be categorized as both.

Power markets favor high efficiency baseload generators with quick, “push-button” start-up capabilities to meet demand peaks. Technologies meeting both criteria has thus far been elusive at a price amenable to the market. Competitive power producers must find a niche of being efficient enough in base generation, or flexible enough in load changing to compete within the market. The dFC-GT, as envisioned, addresses both criteria. As a retro-fit to responsive ‘peaking’ turbines, the dFC-GT has the capability to efficiently produce electricity while the turbine system is idling, while retaining the rapid response capability to balance the electric grid.

This analysis compares the dFC-GT to a simple-cycle GT, a high efficiency combined cycle base-load generator reliant on the grid for transient response, and complete dependence upon the existing electric grid under the cost assumptions of Table 7. Fuel costs represent the US national average for natural gas. Electricity costs comprise energy use and peak demand charges. Applied to this demand profile the annual average cost of energy, including demand charges, is

equivalent to the average US retail electricity price of $0.1041 per kWh [*67*]. Emissions of CO2 from grid sources is also representative of the current US average, though it is expected this emission factor will continue to decline as coal plants are taken off-line. Capacity costs of the CCGT and Peaker plants were taken from standard capacity pricing [*68*], while the dFC-GT was assumed based on GT and SOFC pricing available from EIA and NREL data and literature [*69*].

Table 7 Economic Assumptions [67]

Economic Assumptions		
Variable	Value	Unit
Fuel Costs	4.50	$/MMbtu
Grid Electric Costs	0.050	$/kWh
Peak Demand Costs	3.00	$/kW
Grid Emissions Factor	879.00	lb/MWh
Fuel Emissions Factor	116.39	lb/MMbtu
CCGT Capacity Capital	1500.00	$/kW
Peaker Capacity Capital	750	$/kW
dFC-GT Capacity Capital	2500	$/kW

Figure 25 illustrates the efficiency during off-design operation of a hypothetical 20MW dFC-GT and a 20MW turbine. The off-design performance was calculated from the nominal operating point of the steady-state model presented in Chapter 5. The different technology options will be evaluated for their capability to meet a demand profile representing a large university campus shown in Figure 23. Figure 24 shows a histogram of the demand profile with an overlaid line plot showing the percentage of time a generator of the designated size (10MW, 12MW, etc.) could

meet the demand profile. For this study, the turbine and dFC-GT were sized to 20MW, capable of meeting 98.9%% of the electric demand of Figure 30.

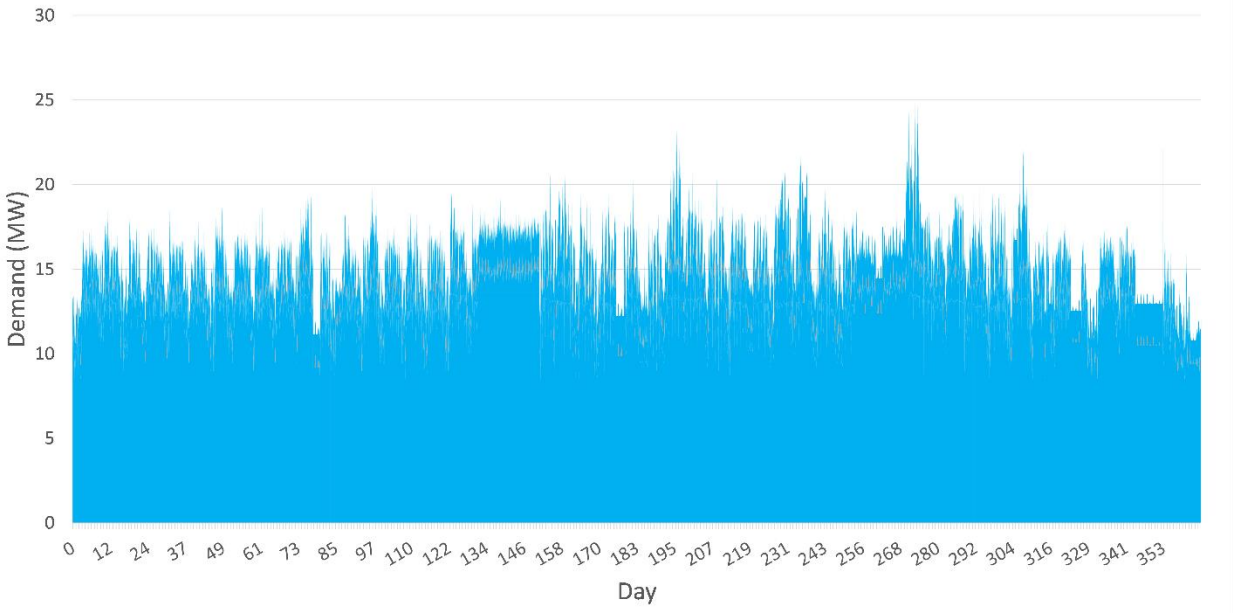

Figure 22 Univ. California Irvine demand profile 2011 (McLarty)

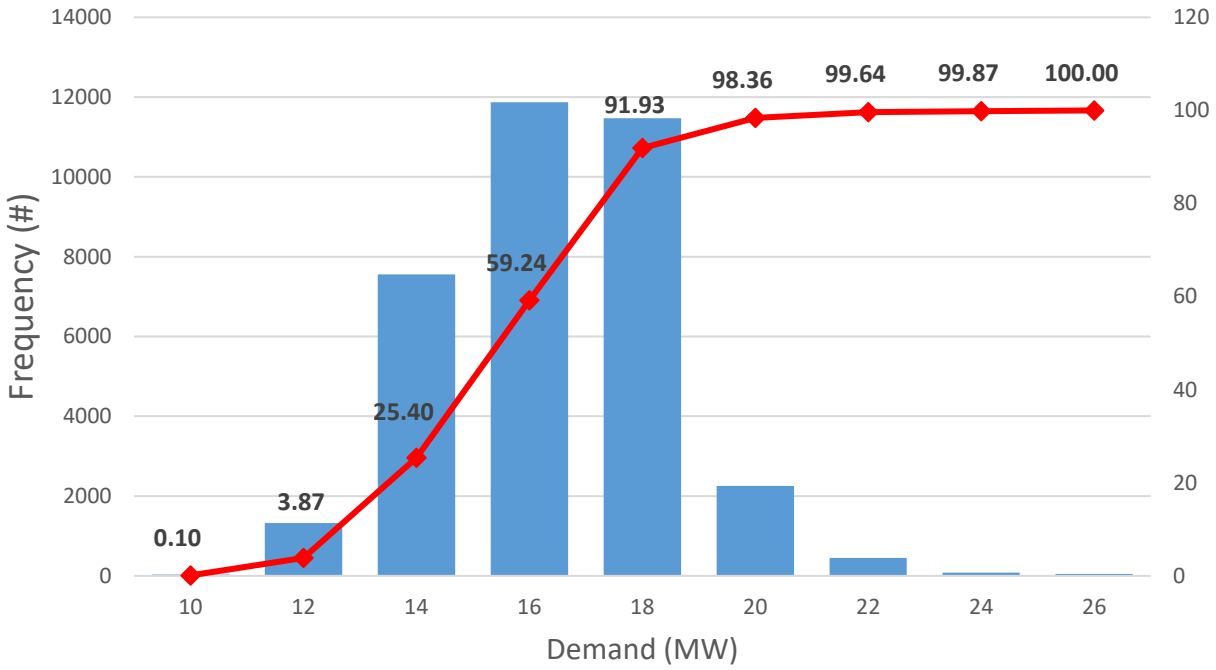

Figure 23 Histogram of Demand Profile

6.1. Comparative Analysis

The standard method for a campus to meet its electric needs is to connect and purchase electricity from the grid. The capital costs of this approach would be common to all 4 approaches, and will therefore not be considered. The total cost of electricity is calculated by Equation 49, with equation 50 representing the grid related emissions. Demand charges are calculated from the monthly peak demand. Tables 8 and 9 outline the costs and carbon emissions for all 4 approaches.

$$\$_{Electric} = kWh_{Grid} \cdot \left(\frac{\$}{kWh_{Grid}}\right) + \left(\frac{\$}{kWh_{Demand}}\right) \cdot Max(kWh_{Grid})_{Month} \quad (57)$$

$$Tons\ {}^{Grid}_{CO_2} = MWh_{Grid} \cdot \frac{lbs}{MWh} \cdot \frac{Tons}{2000lbs} \quad (58)$$

Table 8 Summary of costs and emissions for meeting demand profile

Technology	Capital Financing Costs	On-Site Fuel Costs	Grid energy & demand costs	Total annual costs
Grid dependent	-	-	$7,059,206	$7,059,206
Base-load CC + grid	$953,825	$2,249,604	$2,666,855	$5,870,285
'Peaker' GT	$1,192,281	$5,685,589	-	$6,877,871
dFC-GT	$2,384,563	$3,236,865	-	$5,621,428

Table 9 Summary of Emissions for meeting demand profile

Technology	On-Site Emissions of CO2 (tons)	Grid related Emissions (tons)	Total Emissions (tons)
Grid dependent	-	55,336	55,336
Base-load CC + grid	29,254	19,888	49,142
'Peaker' GT	73,879	-	73,879
dFC-GT	42,079	-	42,079

Baseload power plants operate for long periods of time to meet a constant (base) load. They do not can respond to changes in demand, but have been optimized for high efficiency steady operation. This analysis assumed 55% FTE efficiency for a combined-cycle gas turbine (CCGT) at the 10MW scale. More efficient plants using H-class turbines are available at the 500MW scale. A cost of $1500/kW was assumed from available EIA data. This cost was amortized as a twenty-year investment with a 2.5% financing interest rate. The total monthly payment can be calculated per equation 59.

$$Mortgage = \frac{Interest}{month} \cdot \frac{System\ Size}{1-\left(1+\frac{Interest}{month}\right)^{\#\ months}} \cdot \#Years \qquad (59)$$

For the given demand profile, a continuous load of 10MW could be met by this type of generator, with the balance met by the electric grid. The fuel costs needed to run the 10 MW CCGT utilized equation 60 and an assumed fuel price of $4.50 per MMbtu:

$$\$_{fuel} = \frac{(MW_{electric} \cdot Hours)}{\eta_{electric}} \cdot \frac{293.297 MMbtu_{fuel}}{MWh_{electric}} \cdot \frac{\$}{MMbtu_{fuel}} \quad (60)$$

Emissions were calculated separately for CCGT and the grid imports using the grid emissions factor and fuel emissions factor from Table 7:

$$Tons\ {}^{Fuel}_{CO_2} = MWh_{Gen} / (\frac{293.297 MMbtu}{MWh_{Gen}} \frac{lbs}{MMbtu} \cdot \frac{Tons}{2000 lbs}) \quad (561)$$

Peaker plants are fast ramping generators that often idled until such time that the demand exceeds the baseload and other generation devices. Because they are "turned on" sparingly, the price per kW or MW is significantly higher than baseload generation [*69*]. Variability in both peak demand and local utility rates make the efficiency of peaking plants an afterthought to most power suppliers. Peaking plants are often simple cycle gas turbines as they are easy to build, maintain, and can respond to load changes rapidly.

Current models of gas turbines used in 'peaker' configurations are listed as having ramp-up times of approximately 10 minutes and operate for an average of 15 minutes [*70*] to a few hours. The system cost of the peaker plant listed in Table 7 is $750/kW, significantly less expensive than the higher efficiency CCGT generator. The 'peaker' can meet the demand profile with 28% lower cost than utilizing a CCGT and the grid. The low efficiency operation produces an additional 33% CO2 emissions.

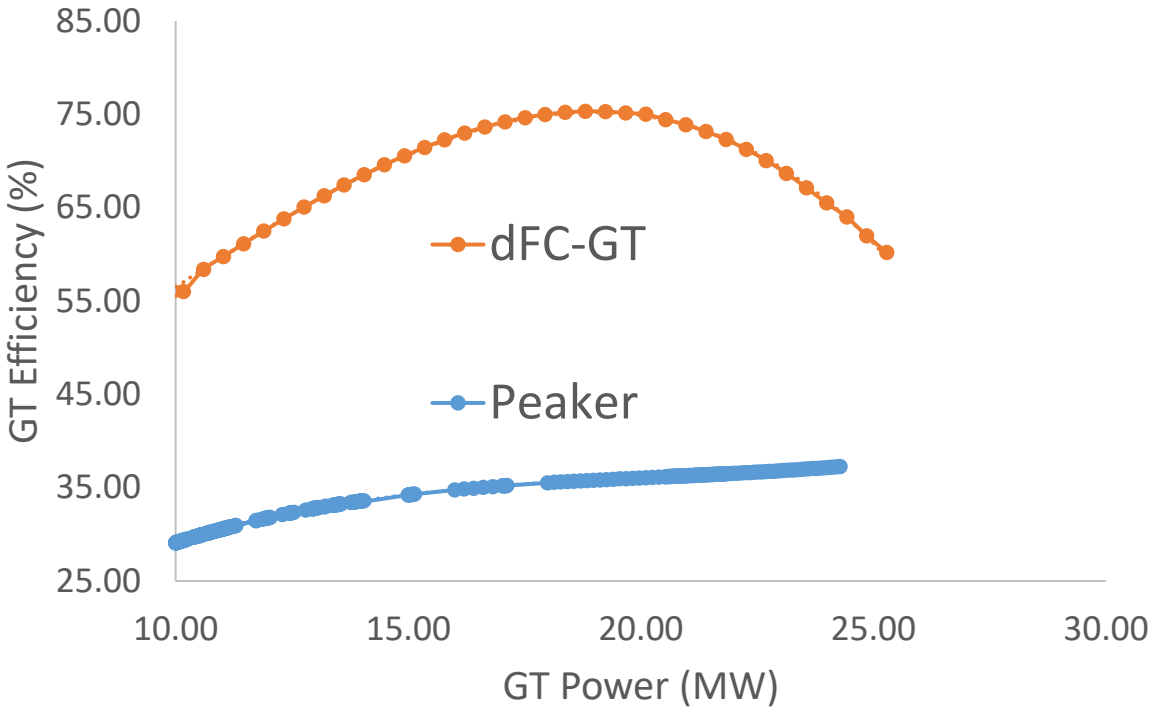

Figure 24 Simple Cycle 'Peaker' and dFC-GT Efficiency Curves

Figure 25 shows the efficiency curve of a 20 MW 'peaker' that operates between 27-38% efficiency combined with the generated efficiency curve of the dFC-GT which operates between 50% and 76%. Depending on the system output and efficiency, a range of possible carbon emissions and power costs is possible. Over the course of its operating range, the dFC-GT can meet the demand profile of Figure 23 above 65% FTE efficiency. That is a significant improvement over current heat engine generation systems.

The dFC-GT configuration is envisioned as a retro-fit to existing gas turbine engines. In this sense, the system could act as a replacement for 'peaking' plant configurations, albeit with considerably higher FTE efficiency as shown in Figure 22. Using the pricing for the CCGT, the 'peaker' generator, and standard pricing for fuel cells from the DOE [*69*], the system cost is assumed to be $2500/kW. The dFC-GT capacity pricing is higher than both the CCGT and peaker

plant, but operating at much higher efficiencies keeps the annual costs lower than both. With the ability to co-produce hydrogen, this cost could be lowered even further by supplying a new revenue stream for power suppliers.

6.2. Distributed Generation

The dFC-GT may also excel in distributed generation for micro-grid arrangements such as college campuses, office parks etc. Distributed generation (DG) is the implementation of power generating technologies by consumers to reduce their grid load and demand charges [*70*]. Peak load times allow customers to generate their power needs through their own systems, while off-peak times allow the customer to send energy back to their local utility, reducing the load on the utility and providing compensation for the consumer [*71*]. Large DG systems are usually linked in such a fashion that they become known as Micro-Grids. Micro-Grids are discrete energy systems consisting of DG systems and separate from the utilities grid. Implementation of a Micro-Grid can occur anywhere from a college campus, to hospitals, to whole city blocks.

Current micro-grids rely on a combination of demand management, energy storage, and some form of generation on site – usually a CHP system [*53*]. These systems are meant to operate independently, if not parallel to the existing utility grid. Analysis and optimization of micro-grids factor in building type, climate, utility costs, and desired generation and/or storage.

Micro-Turbines (pressure ratios < 5) have traditionally been applied to micro-grids as CHP systems, generating power from the turbine and using excess heat to boilers, heating elements etc. [*7*]. From the design study conducted in Chapter 6, the dFC-GT could be applied to DG systems as a power generating device. Although it loses the ability as a CHP system - recycling its

own waste heat for turbine operation - the benefits of increased efficiency could potentially save in both cost and environmental impact. The micro-dFC-GT would maintain the load response of a classic micro-GT and integrate into DG systems as one as well.

6.3. Economic Conclusions

Expanding the renewable and green energy movement requires first that current power generating systems optimize their efficiency and generation. The dFC-GT begins that movement by acting as a retro-fit technology. By retro-fitting existing energy devices (gas turbines) the dFC-GT moves our energy producing industry away from fossil fuels and towards cleaner energy such as hydrogen. Although the dFC-GT does not completely reduce our reliance on “dirty energy,” it takes some of the first steps, benefitting consumers, utilities, and the economy. Coupled with the ability to act as a distributed generation system for micro-grids, and the ability to expand the hydrogen economy, the dFC-GT has a bright outlook should researchers and companies continue to push the technology forward.

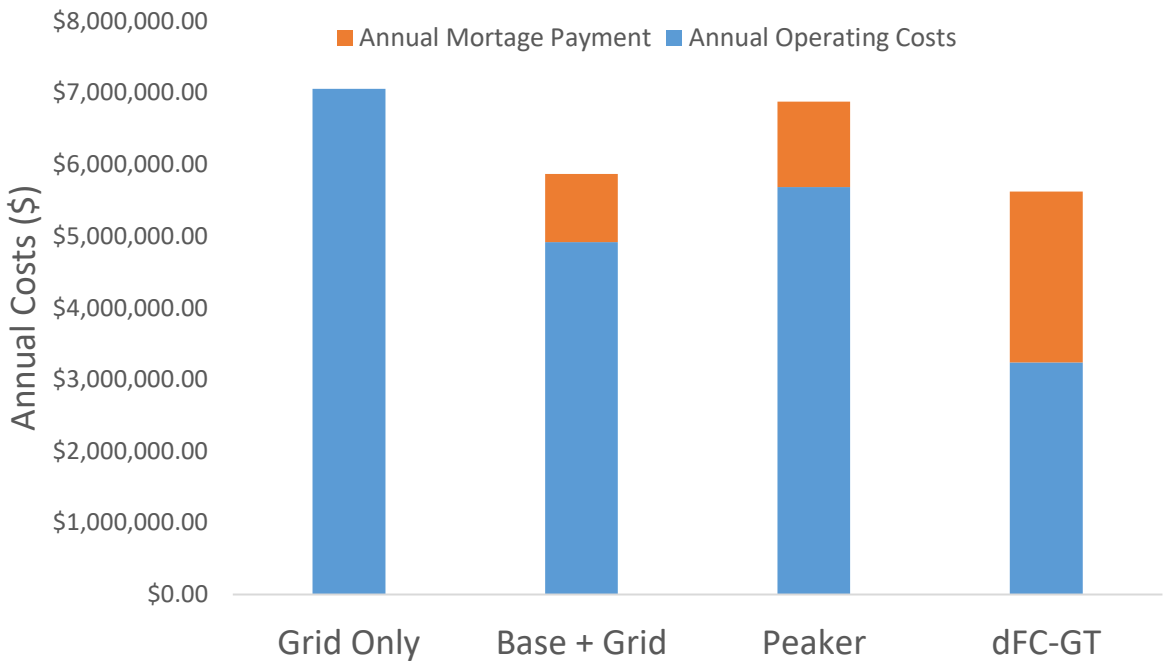

Figure 25 Total Costs of Generation Systems

Figure 26 shows the total costs of each generator annually. Although the mortgage payment for the dFC-GT is higher than both the baseload generator and peaker, the costs are offset by low annual operating costs. Figure 27 shows the monthly emissions by each generator in meeting the UCI demand profile. The dFC-GT can outperform the 'peaker' generator in meeting the demand profile at reduced carbon emissions. The dFC-GT also outperforms baseload generation at 55% efficiency in emissions. Current FC-GT hybrid costs are more expensive than the assumptions taken in this thesis. The goal of this study is to show that in the relative short-term if the trends of cheaper manufacturing continue the dFC-GT is a cost-effective system that will be competitive in the power sector.

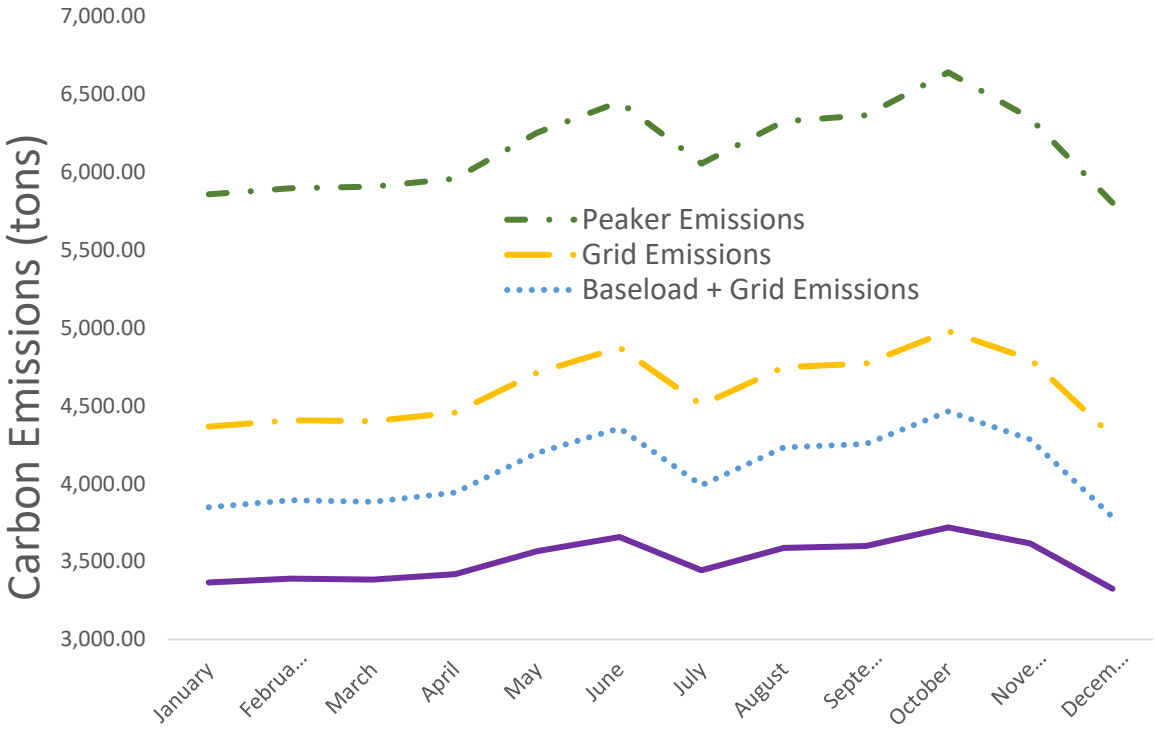

Figure 26 Emissions Comparison of Generation Systems

7. Outlook

The analysis of a dFC-GT relied on two unproven elements of the technology, specifically operation of an SOFC in a thermally sustaining mode, and operation with a pure oxygen cathode. Studies for undersea warfare have evaluated pure oxygen cathodes, but results are not publicly available. Public validation of these two technology elements can be conducted using the pressurized SOFC test stand recently constructed at the Clean Energy Systems Integration lab (CESI) at Washington State University. The test stand is equipped to obtain data from a variety of fuel cell manufacturers under different pressure and temperatures, and oxygen partial pressures. The experimental validation should consider at a minimum the following:

1) *Validation of oxygen partial pressure impacts on cell performance*

The dependence of voltage on operating pressure is well documented for small SOFC button cells, and for tubular SOFC, though significant deviation exists between experiments. Providing analysis of operating voltage for commercial scale planar SOFC at pressure ranges of 1-10bar and oxygen concentrations of 5%-100% can significantly contribute to the public understanding of SOFC pressurization. Initial tests with a "simulated" air-mixture of oxygen and nitrogen will provide a baseline operating condition at a temperature range of 600-800K. Subsequent tests at elevated pressure and oxygen concentration will isolate the impact of reactant concentration and partial pressure.

2) *Validation of thermally balanced pressurized SOFC operation*

Previous experiments cite engineering challenges in maintaining stack temperature in pressurized environments. Utilizing cold-air bypass and/or a series of heat exchangers and other ancillary equipment has been used to maintain thermal stability in FC-GT systems. The system

proposed in this study utilizes endothermic steam reformation internally to balance the thermal energy of the SOFC stack. Investigation and analysis of fuel cell stack thermal gradients can contribute to a greater understanding of thermal energy in fuel cell systems. Research and experiments into pressurized steam reformation can open more opportunities as to how to balance thermal energy in fuel cell systems.

In addition to experimentation being conducted at Washington State University, the dFC-GT introduced a new component to the typical FC-GT arrangement. The Oxygen Transport Membrane (OTM) de-coupled the inlet air stream to the system to direct a pure oxygen feedstock to the cathode of the SOFC. OTM's have been used by manufacturers such as Praxair and Air Products to produce and sell pure oxygen gas. Integration of these components into gas turbine systems has only been conceptualized in design phases thus real-world experimentation can have significant impact on FC-GT research. Experimentation of OTM's should – at minimum – validate the mechanism for oxygen separation. This separation relies on pressure gradients as described in Equations __ and __. Operation at low and intermediate pressures has the potential to limit the oxygen permeability of the OTM. This makes integration with smaller GT or FC-GT systems infeasible.

Finally, the transient response of the system must be investigated. Current FC-GT studies cite slow start-up and/or turn down times in systems. The steady state model presented in this study demonstrated the system's ability to act as a hybrid system while not affecting the turbine mass flow response. This defining characteristic of the dFC-GT should be investigated to validate

the steady state model and continue dFC-GT development. A small (sub-MW) gas turbine may need to be purchased for experiments.

8. Conclusions

This study introduced an alternative fuel cell gas turbine hybrid (FC-GT) arrangement, called a de-coupled fuel cell gas turbine hybrid. The objectives in characterizing the dFC-GT hybrid were met with the following conclusions.

1) The steady-state performance of a dFC-GT was analyzed using first principle mass and energy balances of each component.
2) Nominal operating efficiency was determined to be 75.4%. This nominal operating condition was identified by specifying a nominal current density, 0.5 A/cm2, and nominal area-specific resistance of the fuel cell, .25 A/cm^2 The operating envelope spanned from a minimum current density of 0.105A/cm2 to a maximum of 1.5 A/cm2. The lower current density limit was determined to be a limiting variable of these operating conditions because the local Nernst potential at the end of the anode channel would equal the operating voltage. Thus no further reductions in current would be made under the thermally balanced operating constraint of the Oxy-FC. Recovering 50% of the system's incoming oxidant allowed SOFC operation at a voltage of .936 Volts. A nodal fuel cell model showed 74% of hydrogen was utilized in the fuel cell at nominal conditions. The remaining hydrogen expelled from the fuel cell contained sufficient thermal energy to hybridize with a gas turbine with turbine inlet temperature (TIT) of 1200K. The hybrid system retained greater than 60% efficiency down to 53% of nominal power.
3) De-coupling the fuel cell from the working fluid of the gas turbine allows for greater flexibility in operating conditions. Benefits of de-coupling the system include

additional controls through the back pressure of the OTM, enabling the system to be envisioned as a retrofit technology. Additional benefits include reduced risk of turbomachinery stall, pressurization of the Oxy-FC. Internally reforming a hydrocarbon fuel in the Oxy-FC presents the opportunity for hydrogen recovery. Significant concentrations of hydrogen in the anode exhaust creates the possibility for hydrogen co-production. A 20% reduction in SOFC operating voltage increased hydrogen concentrations 40% in the anode exhaust. The introduction of heat recuperation allowed the system to be scaled to micro-turbine scale. Recuperated dFC-GT micro-turbines recover waste heat and can achieve similar efficiencies of their large-scale counterparts. Challenges still exist in the balancing of thermal energy, and maintaining the thermal tolerances of the Oxy-FC through endothermic steam reforming.

4) Varying nominal design parameters identified critical design trade-offs, namely, the Oxy-FC component driving system power and efficiency. Current density of the fuel cell remained strongly linked with total system efficiency. Back pressure of the OTM described the operating envelope available for a fixed size fuel cell, but greater efficiency was achieved with larger SOFC's. The pressure ratio of the turbine affected the efficiency of the gas turbine, but also changed the open circuit voltage of the fuel cell driving system efficiency as well.
5) Using EIA and other sources, economic assumptions for fuel costs, demand charges, and generator investment were used to determine the competitiveness of the dFC-GT. This study assumed the steady state model presented functioned in the real world

as-is. As a retro-fit, the design captures the capital of existing infrastructure reducing costs and avoiding early de-commissioning. Operation at 75% efficiency is a significant improvement over current generation devices and reduces fuel costs. The system showed a 34% reduction in fuel costs over a 10MW baseload CCGT with supplemental grid purchases along with a 14% reduction in carbon emissions. A reduction of 43% in both fuel costs and carbon emissions over a simple cycle 'peaker' gas turbine was found as well. Amortizing equipment investment as a twenty year 2.5% financing interest rate showed the dFC-GT system was 5% cheaper annually than a baseload generator and nearly 20% cheaper than the simple cycle 'peaker' annually.

Overall, the design study presented warrants further investigation and experimentation. The dFC-GT's combination of a gas turbine and solid oxide fuel cell connects the past, present, and future in power production. This system will be one step in a long process towards an environmentally friendly, sustaining, energy economy.

9. References

[1] F. Calise, M. Dentice d'Accadia, L. Vanoli, and M.R. von Spakovsky, "Single-Level Optimization of a Hybrid SOFC-GT Power Plant," *Power Sources*, vol. 159, no. 2, pp. 1169-1185, September 2006.

[2] Arnab Choudhury, H. Chandra, and A. Arora, "Application of Solid Oxide Fuel Cell Technology For Power Generation - A Review," *Renewable and Sustainable Energy Reviews*, vol. 20, April 2013.

[3] Annamaria Buonomano, Francesoco Calise, Massimo Dentice d Accadia, Adolfo Palombo, and Maria Vicidomini, "Hybrid Solid Oxide Fuel Cells-Gas Turbine Systems for Combined Heat and Power: A Review," *Applied Energy*, vol. 156, pp. 32-85, 2015.

[4] Jack Brouwer, "Hybrid Gas Turbine Fuel Cell Systems," University of California, Irvine, 2004.

[5] Jack Brouwer and R.A Roberts, "Dynamic Simulation of a Pressurized 220 kW Solid Oxide Fuel-Cell-Gas-Turbine Hybrid System: Modeled Performance Compared to Measured Results," *Fuel Cell Science and Technology*, vol. 3, no. 1, pp. 18-25, August 2005.

[6] David J. White, "Hybrid Gas Turbine and Fuel Cell Systems in Perspective Review," University of California, Irvine, Irvine, 1999.

[7] K. Tomsovic Y. Zhu, "Development of Models for Analyzing the Load-Following Performance of Microturbines and Fuel Cells," *Electric Power Systems Research*, vol. 62, no. 1, pp. 1-11, May 2002.

[8] Yaofan Yi, Ashok D. Rao, Jacob Brouwer, and Scott Samuelson, "Analysis and Optimization of a Solid Oxide Fuel Cell and Intercooled Gas Turbine (SOFC-ICGT) Hybrid Cycle," *Power Sources*, vol. 132, no. 1-2, May 2004.

[9] Jason H. Gross, "THE ISSUE: FUEL CELL TECHNOLOGY," *Joint Legislative Air and Water Pollution Control Conservation Committee*, vol. 1, no. 2, July 2002.

[10] William R Grove, "On the Gaseous Voltaic Battery," *Phillosophycal Magazine and Journal of Science*, vol. 21, no. 3, 1842.

[11] Noriko Hikosaka Behling, *Fuel Cells: Current Technology Challenges and Future Research Needs*, 1st ed.: Elsevier, 2012.

[12] L. Barelli, G. Bidini, F. Gallorini, and S. Servili, "Hydrogen production through sorption-enhanced steam methane reforming and membrane technology: A review," *Energy*, vol. 33, no. 4, April 2008.

[13] Mark C. Williams, Joseph P. Strakey, and Wayne A. Surdoval, "The U.S. Department of Energy, Office of Fossil Energy Stationary Fuel Cell Program," *Power Sources*, vol. 143, no. 1-2, April 2005.

[14] Dustin McLarty, Jack Brouwer, and Scott Samuelson, "Fuel Cell - Gas Turbine Hybrid System Design Part I: Steady State Performance," *Power Sources*, pp. 412-420, November 2014.

[15] Dustin McLarty, Jack Brouwer, and Scott Samuelson, "Hybrid Fuel Cell Gas Turbine System Design and Optimization," *Journal of Fuel Cell Science and Technology*, vol. 10, 2013.

[16] James Larminie, *Fuel Cell Systems Explained*, 2nd ed.: Oxford Brookes University, 2003.

[17] Phillip A Armstrong, "Method for Predicting Performance of an Ion Transport Membrane Unit-Operation," Air Products and Chemicals, Allentown, 2015.

[18] Haihui Wang, Weishan Yang , Cristina Tablet, and Jurgen Caro, "Diffusion Fundamentals: Oxygen Diffusion Through Perovskite Membranes," Physical Chemistry and Electrochemistry, Hanover, Germany, 2005.

[19] Paul N. Dyer, Robin E. Richards, Steven L. Russek, and Dale M. Taylor, "Ion Transport Membrane Technology for Oxygen Separation and Syngas Production," *Solid State Ionics*, vol. 134, no. 1-2, pp. 21-33, October 2000.

[20] V.V Kharton et al., "Perovskite-Type Oxides for High Temperature Oxygen Separation Membranes," *Membrane Science*, vol. 163, no. 2, pp. 307-317, November 1999.

[21] M.A. Nemitallah, M.A. Habib, R. Ben-Mansour, and A.F. Ghoneim, "Design of an Ion Transport Membrane Reactor for Gas Turbine Combustion Application," *Membrane Science*, vol. 450, no. 1, pp. 60-71, January 2014.

[22] Phillip Armstrong, Douglas L. Bennett, Ted Foster, and VanEric Stein, "ITM Oxygen: The New Oxygen Supply for the New IGCC Market," in *Gasification Technologies*, San Fransisco, 2005.

[23] P.S. Maiyaa et al., "Oxygen Transport by Oxygen Potential Gradient in Dense Ceramic Oxide Membranes," *Solid State Ionics*, vol. 99, no. 1-2, August 1997.

[24] Anthony F. Sammells, Michael Schwartz, Richard A Mackay, Thomas F. Barton, and David R. Peterson, "Catalytic Membrane Reactors for Spontaneous Synthesis Gas Production," *Catalysis Today*, vol. 56, no. 1-3, February 2000.

[25] Praxair, *Praxair's Oxygen Transport Membrane Technology for Syngas and Power Applications*. Pittsburgh, PA: Department of Energy, 2015.

[26] Rodney John Allam, "Improved Oxygen Production Technologies," *Energy procedia*, vol. 1, no. 1, February 2009.

[27] E. T Robinson, "Oxygen Transport Membranes for Ultra Clean Fuel Production," Torix Inc., Mentor, 2003.

[28] M.A. Nemitallah and M.A. Habib, "Experimental and Numerical Investigations of an Atmospheric Diffusion Oxy-Combustion Flame in a Gas Turbine Model Combustor," *Membrane Science*, vol. 111, no. 1, pp. 401-415, November 2013.

[29] M.A. Habib, Pervez Ahmed, Rached Ben-Mansour, Hassan M. Badr, and Patrick Kirchen, "Modeling of a Combined Ion Transport and Porous Membrane Reactor for Oxy-Combustion," *Membrane Science*, vol. 446, no. 1, pp. 230-243, November 2013.

[30] Dustin McLarty and Jack Brouwer, "Poly-Generating Closed Cathode Fuel Cell with Carbon Capture," *Applied Energy*, vol. 131, July 2014.

[31] Kasra Nikooyeh, Ayodeji A. Jeje, and Josephine M. Hill, "3D Modeling of Anode-Supported Planar SOFC with Internal Reforming of Methane," *Power Sources*, vol. 171, no. 2, September 2007.

[32] S.K. Park,T.S. Kim, J.H. Kim, J.L. Sohn W.J Yang, "Design Performance Analysis of Pressurized Solid Oxide Fuel Cell/Gas Turbine Hybrid Systems Considering Temperature Constraints," *Power Sources*, vol. 160, no. 1, September 2006.

[33] Severin Borenstein, "The Trouble With Electricity Markets: Understanding California's Restructuring Disaster," *Economic perspectives*, vol. 16, no. 1, February 2002.

[34] Joshua Eichman, Fabian Mueller, Brian Tarroja, Lori Smith-Schell, and Scott Samuelson, "Exploration of the Integration of Renewable Resources into California's Electric System using Holistic Grid Resource Integration and Deployment (HiGRID) Tool," *Energy*, vol. 50, no. 1, February 2013.

[35] Brian Tarroja, Fabian Mueller, Joshua Eichman, and Scott Samuelson, "Metrics For Evaluating The Impacts of Intermittent Renewable Generation On Utility," *Energy*, vol. 42, no. 1, June 2012.

[36] Dongsik Jang, Eom Jiyong, Min Jae Park, and Jae Jeung Rho, "Variability ofElectricity Load Patterns and Its Effect On Demand Response," *Energy Policy*, vol. 88, January 2016.

[37] Wolfgang Winkler, Pedro Nehter, Mark C Williams, David Tucker, and Randy Gemmen, "General Fuel Cell Hybrid Synergies and Hybrid System Testing Status," *Power Sources*, vol. 159, no. 1, pp. 656-666, September 2006.

[38] Tae Won Song, Jeong Lak Sohn, Tong Seop Kim, and Sung Tack Ro, "Performance characteristics of a MW-class SOFC/GT Hybrid System Based on a Commercially Available Gas Turbine," *Power Sources*, vol. 158, no. 1, July 2006.

[39] Dayadeep S. Monder, K. Nandakumar, and Karl T. Chuang, "Model development for a SOFC button cell using H2S as fuel," *Journal of Power Sources*, vol. 162, no. 1, November 2006.

[40] Jens Palsson, Azra Selimovic, and Lars Sjunnesson, "Combined Solid Oxide Fuel Cell and Gas Turbine Systems for Efficient Power and Heat Generation," *Power Sources*, vol. 86, no. 1-2, pp. 442-448, March 2000.

[41] Penyarat Chinda and Pascal Brault, "The Hybrid Solid Oxide Fuel Cell (SOFC) and Gas Turbine (GT) Systems Steady State Modeling," *Hydrogen Energy*, vol. 37, no. 11, pp. 9237-9248, June 2012.

[42] Jason Kupecki, "Considerations Regarding Modeling of MW-scale IG-SOFC Hybrid Power System," Thesis 2009.

[43] Andrew S. Martinez, Jacob Brouwer, and Scott Samuelson, "Feasibility Study for SOFC-GT Hybrid Locomotive Power: Part 1. Development of a Dynamic 3.5 MW SOFC-GT FORTRAN Model," *Power Sources*, vol. 213, Septmeber 2012.

[44] M.L. Ferrari, Matteo Pascenti, Roberto Bertone, and Loredana Magistri, "Hybrid Simulation Facility Based on Commercial 100 kWe Micro Gas Turbine," *Fuel Cell Science and Technology*, vol. 6, no. 3, May 2009.

[45] Nischal Srivastava, "Modeling of Solid Oxide Fuel Cell/Gas Turbine Hybrid System," Mechanical Engineering, Florida State University, Thesis 2006.

[46] Joshua E. Freeh, Louis M. Larosiliere Christopher J. Steffen Jr, "Solid Oxide Fuel Cell/Gas Turbine Hybrid Cycle Technology for Auxiliary Aerospace Power," NASA, Cleveland, OH, 2005.

[47] Fuel Cell Energy Inc., "FCE Power Plant in Eath Day Dedication at Montana Clinic," *Fuel Cells Bulletin*, vol. 2006, no. 6, June 2006.

[48] Fuel Cell Energy Inc., "Record Electric Efficiency for DFC/Turbine Unit," *Fuel Cells Builletin*, vol. 2006, no. 4, April 2006.

[49] F. Mueller, Jack Brouwer, F. Jabbari, and Scott Samuelson, "Dynamic SImulation of an Integrated Solid Oxide Fuel Cell System including Current-Based Fuel Flow Control," *Fuel Cell Science and Technology*, vol. 3, pp. 144-154, October 2006.

[50] A. Palombo, L. Vanoli F. Calise, "Design and partial load exergy analysis of a hybrid SOFC-GT power plant," 2005.

[51] Sue Fuhs, "GE Hybrid Power Generation Systems," 2012.

[52] Hossein Ghezel-Ayagh et al., "State of direct fuel cell/turbine systems development," *Power Sources*, vol. 152, no. 1, pp. 219-225, December 2005.

[53] Environmental Protection Agency, "Economic Impact Analysis of the Stationary Combustion Turbine NSPS: Final Report," 2006.

[54] A Traverso, L. Magistri, and A.F Massardo, "Turbomachinery For the Air Management and Energy Recovery in Fuel Cell Gas Turbine Hybrid Systems," *Energy*, vol. 35, no. 2, February 2010.

[55] Florian Leucht, Wolfgang G. Bessler, Josef Kallo, K. Andreas Friedrich, and H. Muller-Steinhagen, "Fuel Cell System Modeling for Solid Oxide Fuel Cell/Gas Turbine Hybrid Power Plants, Part 1: Modeling and Simulation Framework," *Power Sources*, vol. 196, no. 3, February 2011.

[56] A. F. Massardo Traverso et al., "Transient Modeling of the NETL Hybrid Fuel Cell/Gas Turbine Facility and Experimental Validation," *Engineering for Gas Turbines and Power*, vol. 129, no. 4, pp. 1012-1019, 2007.

[57] Farshid Zabihian and Alan Fung, "A Review on Modeling of Hybrid Solid Oxide Fuel Cell Systems," *International Journal of Engineering*, vol. 3, no. 2, March 2009.

[58] Dustin McLarty, Yusuke Kuniba, Jack Brouwer, and Scott Samuelson, "Experimental and Theoretical Evidence for Control Requirements in Solid Oxide Fuel Cell Gas Turbine Hybrid Systems," *Power Sources*, vol. 209, March 2012.

[59] Jung-Ho Wee, "Molten Carbonate Fuel Cell and Gas Turbine Hybrid Systems as Distributed Energy Resources," *Applied Energy*, vol. 88, no. 12, December 2011.

[60] Stephen J. McPhail, Anja Aarva, Hary Devianto, Roberto Bove, and Angelo Moreno, "SOFC and MCFC: Commonalities and Opportunities for Integrated Research," *Hydrogen Energy*, vol. 36, no. 16, August 2011.

[61] P. Aguiar and L. Kershenbaum, "Modeling of an Indirect Internal Reforming Solid Oxide Fuel Cell," *Chemical Engineering Science*, vol. 57, no. 10, May 2002.

[62] Prapan Kuchonthara, Sankar Bhattacharya, and Atsui Tsutsumi, "Energy Recuperation in Solid Oxide Fuel Cell (SOFC) and Gas Turbine (GT) Combined System," *Power Sources*, vol. 117, no. 1, pp. 7-13, May 2003.

[63] J. Sunarso et al., "Mixed Ionic-Electronic Conduction (MIEC) Ceramic-Based Membranes for Oxygen Separation," *Membrane Science*, vol. 320, no. 1, pp. 13-41, March 2008.

[64] Laurence Meixner et al., "Electrochemical Oxygen Separation Using Solid Electrolyte Ion Transport Membranes," Air Products and Chemicals Inc., Allentown PA, 2002.

[65] Raymond A. Cutler et al., "Solid Electrolytes and Electrical Interconnects for Oxygen Delivery Devices," *Solid State Ionics*, vol. 176, no. 35-36, pp. 2589-2598, November 2005.

[66] Neha Rustagi, Amgrad Elgowainy, and Erika Gupta, "Hydorgen Delivery Cost Projections - 2015," Department of Energy: Hydrogen and Fuel Cells Program Record, 2016.

[67] U.S. Energy Information Administration. (2017, February) Independent Statistics and Analysis: EIA. [Online]. http://www.eia.gov/electricity/data/browser/#/topic/7?agg=2,0,1&geo=g&freq=M&start=200101&end=201611&ctype=linechart&ltype=pin&rtype=s&maptype=0&rse=0&pin=

[68] Victor deBiasi, "Combined cycle heat rates at simple cycle $/kW plant costs," Gas Turbine Wrold, 2013.

[69] Energy Information Association, "Analysis of the Impacts of the Clean Power Plant," 2015.

[70] A. Zhuk, Yu Zeigamik, E. Buzoverov, and A. Sheindlin, "Managing Peak Loads In Energy Grids: Comparative Economic Analysis," *Energy Policy*, vol. 88, no. 1, January 2016.

[71] N. Javaid, I. Khan, M. N. Ullah, A. Mahmood, and M. U. Farooq, "A Survey of Home Energy Management Systems in Future Smart Grid Applications," 2012.

10. Appendices

10.1. MatLab© Code

The following is the code used to generate the dFC-GT system:

10.1.1. Steady State system

```
function
[Efficiency,Eff_FC,Eff_GT,W_net,Wfc_vec,W_gt,Wc2,T_out,FCFlowOut,FC_Fuel_vec,combustorCH4,ReactMix,V_ve
c,Utilization,R_actual,Rt,recovery,Qextra,i_array,recirc_vec,nO2] = dFC_GT(varargin)

Tin = varargin{1};                %Temp, Composition, Flow in to system
Pr = varargin{2};                 %Pressure Ratio across turbomachinary
P_ITMperm = varargin{3};          %Back pressure of OTM
TIT = varargin{4};                %Ideal Turbine Inlet Temp
M_air = varargin{5};              %Mass Flow Rate of GT In
iDen = varargin{6};               %Total Current Density of FC
Air.O2 = .21;  %Oxygen concentration of air
Air.N2 = .79;  %Nitrogen concentration of air

if length(varargin)>6
   recovery = varargin{7};        %run at constant value of recovery
else recovery = ones(length(Tin),1).*.51; %Intial value of recovery
end
Cogen = 0;                %Decide whether hydrogen will be generated
S2C = linspace(2,2,length(Pr))';   %Design steam to carbon ratio
TurbEff = linspace(.88,.88,length(Pr))';   %Turbine Efficiency
CompEff = linspace(.8,.8,length(Pr))';     %Compressor Efficiency
LHVH2 = 240420;                   %Lower Heating Value of H2
vectorLength = max([length(Pr), length(P_ITMperm),length(TIT)]);
LHVfuel = zeros(vectorLength,1)+802301; %Lower heating value of CH4
TIT = zeros(length(TIT),1)+TIT;
%% Compressor
MMass = MassFlow(Air)/NetFlow(Air); %MolarMass flow of air
spec = fieldnames(Air);
for i = 1:1:length(spec)
   CompFlow.(spec{i}) = Air.(spec{i})*M_air/MMass; %Molar inlet flow to system
end
CompFlow.T = Tin;  %Inlet flow temp
T1 = Tin;
n = length(T1);
Pin = ones(n,1).*101;  %Inlet pressure
[Wc1,T2,P2] = compress_struc(CompFlow,CompEff,Pr,Pin); %Compressor Model
CompFlow.T = T2;   %Temperature out of compressor
error = 100;
while max(abs(error))> 1e-4 %loop to solve for TIT by varying the recovery percentage of o2
   B = find(recovery>.99); %Don't allow recovery over 100%
if ~isempty(B)
   recovery(B) = 1;
end
%% OTM for Oxygen Separation
```

```
[NonPerm,O2Flow,Q_preheat,R_actual,Rt] = ITM_struc(CompFlow,P2,P_ITMperm,recovery); %ITM Model
%% Parasitic Compressor
Pr2 = (Pr.*Pin+25)./P_ITMperm;     %Initialization for parasitic compressor to FC
O2Flow.T = 320;                %cooling back to near ambient conditions
[Wc2,T5,P5] = compress_struc(O2Flow,CompEff,Pr2,P_ITMperm);   %Compressor2 Model
%% Initialization to Fuel Cell
L = 10;    %Length of cells
W = 10;    %Width of cells
nodes = 10; %Nodes to analyze
F = 96485;
%Initialize output matrices
i_array = zeros(nodes,n);
recirc_vec = zeros(n,1);
FC_Fuel_vec = zeros(n,1);
V_vec = zeros(n,1);
Wfc_vec = zeros(n,1);
Utilization = zeros(n,1);
FCFlowOut=[];
Q_HVanodeOut = zeros(n,1);
FCFlowOut.T = zeros(n,1);
FCFlowOut.H2 = zeros(n,1);
FCFlowOut.H2O = zeros(n,1);
FCFlowOut.CO = zeros(n,1);
FCFlowOut.CO2 = zeros(n,1);
FCFlowOut.CH4 = zeros(n,1);
%% Fuel Cell Model
for k = 1:1:n
      Supply.O2 = O2Flow.O2(k);   %Inlet oxidant to FC
%# of cells will determine current density and thus voltage !!
Cells = O2Flow.O2(k)./(iDen(k)*L*W/(4000*F));
%Cells = [510000];    %Constant Cell size
Cells_vec(k,:) = Cells;
[i,recirc,FC_Fuel,FlowOut,V,W_fc,U] = FuelCell_struc(1023,.25,.6,S2C(k),Supply,L,W,nodes,Cells,Pr(k)); %FC model
i_array(:,k) = i;
recirc_vec(k) = recirc;
FC_Fuel_vec(k) = FC_Fuel;
V_vec(k) = V;
Wfc_vec(k) = W_fc;
Utilization(k) = U;
FCFlowOut.T(k) = FlowOut.T;
FCFlowOut.H2(k) = FlowOut.H2;
FCFlowOut.H2O(k) = FlowOut.H2O;
FCFlowOut.CO(k) = FlowOut.CO;
FCFlowOut.CO2(k) = FlowOut.CO2;
FCFlowOut.CH4(k) = FlowOut.CH4;
Q_HVanodeOut(k) = FlowOut.H2*241826.4 + FlowOut.CO*283004.7 + FlowOut.CH4*802301;%LHV of anode off
products
end
%% Combustor Model
[ReactMix, Qextra] = combust_struc(NonPerm,FCFlowOut,Q_preheat,TIT);
combustorCH4 = Qextra./LHVfuel; %If excess fuel is needed
```

```
combustorCH4(combustorCH4<0) = 0;
H2co_produced = -Qextra./LHVH2; %If H2 produced
H2co_produced(H2co_produced<0) = 0;
if length(varargin)<7   %% Adjust recovery to meet TIT
      a = .25;
      error = Qextra./(FC_Fuel*LHVfuel);
  newrecov = (1-a)*recovery + a*(recovery + error);
  recovery = min(newrecov,1);
  error(newrecov>=1) = 0;
else %% Run at constant recovery
      error = 0;
end
end
%% Turbine Model
[Wt,T_out,TurbFlow] = turbine_struc(ReactMix,TurbEff, 1./Pr);
%% Results
nO2 = O2Flow.O2;
W_gt = Wt-Wc1;                    %Gas turbine power minus compression%
Eff_FC = Wfc_vec./(FC_Fuel_vec.*LHVfuel);
Eff_GT = (Wt-Wc1)./(Q_HVanodeOut + combustorCH4.*LHVfuel H2co_produced.*LHVH2); %Efficiency of Gas
Turbine
W_net = Wfc_vec + W_gt - Wc2;  %Net power output of hybrid
%% Decide whether cogeneration of h2 is wanted
if Cogen == 0
   Efficiency = (W_net)./((FC_Fuel_vec + combustorCH4).*LHVfuel); %Hybrid Efficiency without cogeneration
else
   Efficiency = (W_net+H2co_produced*LHVH2)./((FC_Fuel_vec + combustorCH4).*LHVfuel);%hybrid efficiency
with cogeneration
end
```

10.1.2. Compressor/Turbine

```
function [Wc, Tout, P2] = compress_struc(Flow, eff, Pr, Pin)
%% Inlet Conditions
Ru = 8.314;
P2 = Pr.*Pin;
[~,Hin] = enthalpy2(Flow);
Tin = Flow.T;
Tavg = (Tin+Pr.^(1-1/1.4).*Tin)/2;
Flow.T = Tavg;
Cp = SpecHeat2(Flow);
gam = Cp./(Cp-Ru);
FlowS = Flow;
FlowS.T = Pr.^(1-(1./gam)).*Tin; %Isnetropic Temperature Change
[~,Hs] = enthalpy2(FlowS); %Isentropic Enthalpy change
%% Actual Enthalpy Change
Hout = Hin + 1./eff.*(Hs-Hin);
Tout = Tin + 1./eff.*(FlowS.T-Tin);
T_error = Tin*0+ 100;
%% Solve for Temp out
while min(abs(T_error)) > .1
   Flow.T = Tout;
   [~,Hguess] = enthalpy2(Flow);
   T_error = (Hout - Hguess)./(Cp.*NetFlow(Flow));
   Tout  = Tout + T_error; %Reiteration to calculate temperature out
end
%% Power Out
Wc = Hout - Hin; %power taken for compression


function [Wt,Tout,Flow] = turbine_struc(Flow,EffTurb, Pr)
%% Inlet Conditions
Ru = 8.314;
Tin = Flow.T;
[~,Hin] = enthalpy2(Flow);
Tavg = (Tin+Pr.^(1-1/1.4).*Tin)/2;
Flow.T = Tavg;
Cp = SpecHeat2(Flow);
gam = Cp./(Cp-Ru);
FlowS = Flow;
FlowS.T = Pr.^((gam-1)./gam).*Tin;   %Isentropic Expansion Temperature
[~,Hs] = enthalpy2(FlowS);    %Isentropic enthaplpy out
%% Actual Enthalpy Change
Hout = Hin-EffTurb.*(Hin-Hs);         %Actual enthalpy out
Tout = Tin - EffTurb.*(FlowS.T - Tin);
T_error = Tin*0 +100;
%% Solve for Temp Out
while min(abs(T_error)) > .1      %Reiteration to calculate temperature out
   Flow.T = Tout;
   [~,H_guess] = enthalpy2(Flow);
   T_error = (H_guess-Hout)./(Cp.*NetFlow(Flow));
```

```
   Tout = Tout - T_error;
end
%% Power Out
Wt = Hin - Hout;      %Isentropic expansion power generation
Flow.T = Tout;
```

10.1.3. Oxygen Transport Membrane

```
function [NonPermeate,Permeate,Q_preheat,R_actual,Rt] = ITM_struc(Flow,Pin,P_ITMperm,recovery)
%% Inputs to OTM
T = Flow.T;
Hin = enthalpy2(Flow);      %Enthalpy in from compressor
 %% Required Preheating
T_preheated = max(T,1073);
Flow.T = T_preheated;
Hheated = enthalpy2(Flow);
Q_preheat = (Hheated)-(Hin);
%% Output Conditions
Tout = T_preheated;
TO2 = T_preheated;
Permeate.T = TO2;
NonPermeate.T = Tout;
X_O2 = Flow.O2./NetFlow(Flow);
%% Recovery of Oxygen
Rt = 1-(1-X_O2).*P_ITMperm./(X_O2.*(Pin-P_ITMperm));%Theoretcial O2 recovery(Air Prod)
R_actual = max(0,(recovery) .* Rt); %(Actual O2 Recovery)
NO2 = (R_actual).*Flow.O2; %Molar Flow O2
Permeate.O2 = NO2;
%% Non-permeate to Combustor
NonPermeate.O2 = Flow.O2-NO2; %Molar flow of Non-Permeate
NonPermeate.N2 = Flow.N2;
NonPermeate.T = T_preheated;
end
```

10.1.4. Combustor

```
function [ReactMix, Qextra] = combust_struc(Air,Fuel,Q,TIT)
NetIn =[];
Hair = enthalpy2(Air);
Hanode = enthalpy2(Fuel);
spec = fieldnames(Air);
spec = spec(~strcmp(spec,'T'));
for i = 1:1:length(spec)
   NetIn.(spec{i}) = Air.(spec{i});
end


spec2 = fieldnames(Fuel);
spec2 = spec2(~strcmp(spec2,'T'));
spec = unique([spec;spec2]);
for i = 1:1:length(spec2)
   if ~isfield(NetIn,spec2{i})
      NetIn.(spec2{i}) = Fuel.(spec2{i});
   else NetIn.(spec2{i}) = NetIn.(spec2{i}) + Fuel.(spec2{i});
   end
end
%% 3 reaction:
% CH4 + 1.5O2 --> CO + 2H2O
% CO + .5O2 --> CO2
% H2 + .5O2 --> H2O
R.CH4 = NetIn.CH4;
R.CO = (NetIn.CO+R.CH4);
R.H2 = NetIn.H2;
sumR = 1.5*R.CH4 + 0.5*R.CO + 0.5*R.H2;
r = fieldnames(R);
phi = sumR/NetIn.O2;
if phi>1 %rich combustion
   for i = 1:1:length(r)
      R.(r{i}) = R.(r{i})/phi; %rich combustion limited by O2
   end
end
for i = 1:1:length(spec)
   if strcmp(spec{i},'CH4')
      ReactMix.CH4 = NetIn.CH4 - R.CH4;
   elseif strcmp(spec{i},'CO')
      ReactMix.CO = NetIn.CO + R.CH4- R.CO;
   elseif strcmp(spec{i},'CO2')
      ReactMix.CO2 = NetIn.CO2 + R.CO;
   elseif strcmp(spec{i},'H2')
      ReactMix.H2 = NetIn.H2  - R.H2;
   elseif strcmp(spec{i},'H2O')
      ReactMix.H2O = NetIn.H2O + 2*R.CH4 + R.H2;
       elseif strcmp(spec{i},'O2')
      ReactMix.O2 = NetIn.O2 - 1.5*R.CH4 - .5*R.CO - .5*R.H2;
   else
      ReactMix.(spec{i}) = NetIn.(spec{i});
```

```
    end
end
Qextra = zeros(length(TIT),1);
if ~isempty(TIT)
    ReactMix.T=TIT;
    Hout = enthalpy2(ReactMix);
    Qextra = Hout - Hair  - (Hanode - Q);
else
    ReactMix.T =  zeros(length(Air.T),1)+1000;
    T_error = 100;
    while min(abs(T_error) > .001)
      Hout = enthalpy2(ReactMix);
      Cp = SpecHeat2(ReactMix);
      T_error = (Hair + (Hanode - Q) - Hout)./(Cp.*NetFlow(ReactMix));
      ReactMix.T = ReactMix.T+T_error;
    end
end
```

10.1.5. Fuel Cell

```
function [i,r,FuelFlow,FlowOut,V,P,Utilization] = FuelCell_struc(T,ASR,e2,S2C,Oxidant,L,W,n,Cells,Pr)
Ru = 8.314;
F = 96485; %Faraday constant C/mol
Oxidant.O2 = Oxidant.O2./Cells;
Oxidant.T = T;
J = 4000*F*Oxidant.O2; % total current in A/cell
V = .85;
%%Initial guesses
r = .5;
h = enthalpy2(298);
hrxn1 = 2*h.H2O-2*h.H2-h.O2; %2H2 + O2 -->  2H2O
hrxn2 = h.CO2+h.H2-h.CO-h.H2O; %CO + H20 --> CO2 + H2
hrxn3 = 3*h.H2+h.CO-h.CH4-h.H2O; %CH4+H2O --> CO + 3H2
Qgen = -hrxn1*Oxidant.O2 - J*V/1000; %total heat released in kW/cell
Qcool = hrxn3 + e2*hrxn2; %cooling in kJ/kmol of CH4
Fuel.CH4 = Qgen./Qcool; %flow rate in kmol/sec-cell
h = enthalpy2(T);
s = entropy2(T);
E0 = -((h.H2O-s.H2O.*T)-(h.H2-s.H2.*T)-.5*(h.O2-s.O2.*T))/(2*F); %reference voltage
%solve for distribution
i = (ones(n,1)).*(J./(L.*W)); %Initial current distribution per cell
J_int = zeros(n,1);
error = 1;
while abs(error)>1e-3
   r = S2C/((.5*S2C-1)*(1+e2)+2*Oxidant.O2/Fuel.CH4);
   for k=1:1:n
      J_int(k) = sum(i(1:k))*(W*L/n); %integral of current density as function of length, total current thus far
   end

   X_H2 = 1+e2/3-2*Oxidant.O2*r/(3*Fuel.CH4)-(1-r)/(6000*F*Fuel.CH4)*J_int;
   X_H2O = 2*Oxidant.O2*r/(3*Fuel.CH4) - (1+e2)/3 + (1-r)/(6000*F*Fuel.CH4)*J_int;
   X_CO_L = (1-e2)/3;
   X_CO2_L = 1 - X_CO_L - X_H2(end) - X_H2O(end);
   SteamRatio = X_H2O(end)*3*Fuel.CH4*r/(1-r)/(Fuel.CH4+0.5*X_CO_L*3*Fuel.CH4*r/(1-r));
   E = E0 + Ru*T/(2*F)*log(X_H2./X_H2O.*Pr.^.5);%Nernst Potential
   error2 = 1;
   count=0;
   if error == 1
      V = mean(E - i*ASR);
   end
   while abs(mean(error2))>(J*1e-6) || count < 2
      i = max(0,(E-V)/ASR);%new current distribution
      error2 = (sum(i)/n*L*W) - J;%error in total current
      V = V + .5*(error2/(L*W)*ASR) ;
      count = count + 1;
   end
   Qgen = -J/(4000*F)*hrxn1 - V*J/1000;%heat release from electrochemistry
   NewFuel = Qgen/(e2*hrxn2+hrxn3); %energy balance heat generated = reformer cooling
   error = (Fuel.CH4-NewFuel)/Fuel.CH4; %change in fuel estimation on this iteration
```

```
    Fuel.CH4 = .8*Fuel.CH4+.2*NewFuel;
end
FuelFlow = Fuel.CH4*Cells;
FlowOut.T = T;
FlowOut.H2 = X_H2(end)*3*Fuel.CH4*Cells;
FlowOut.H2O = X_H2O(end)*3*Fuel.CH4*Cells;
FlowOut.CO = X_CO_L*3*Fuel.CH4*Cells;
FlowOut.CO2 = X_CO2_L*3*Fuel.CH4*Cells;
FlowOut.CH4 = 0;
Utilization = J/(2000*F)/(4*Fuel.CH4); %actual H2 use in kmol/s divided by ideal H2 production in kmol/s
P = (V*J)/1000*Cells;
```

10.2. Derivations of Nodal FC Mode Equations

The following are derivations used to obtain equations 31-45 in the Fuel Cell model

Variable	Symbol	Units
Total Current	*J*	*amps*
Molar Flow Rate	$\dot{n}$	*mol/sec*
Faraday's Constant	*F*	*Joule/Mol*
Current Density	*I*	*amp/cm²*
Width of Fuel Cell	*W*	*cm*
Length of Fuel Cell	*L*	*cm*
Total Molar Flow	$\dot{N}$	*mol/sec*
Recirculation	*r*	-
Water-Gas Shift Effectiveness	ε_{WGS}	-
Concentration	*X*	-
Area	*A*	*cm²*
Voltage	*V*	*Volts*
Heat of Reaction	Δh_f^0	*J/mol*

Total Current in FC:

$$J = \dot{n}_{O_2} \cdot 4F$$

Total current density along length of cell:

$$\int_0^L i(x) \cdot W \cdot dx$$

Mass balance:

$$\dot{N}_{anode,in} = \dot{N}_{anode,out} = \frac{3\dot{N}_{CH_4}}{(1-r)}$$

$$\dot{n}_{H_2}(x) = (\dot{n}_{H_2})_{in} - \int_0^x \frac{i(x)}{2F} \cdot W dx$$

$$(\dot{n}_{H_2})_{in} = (3 + \varepsilon_{WGS})\dot{N}_{CH_4} + \dot{n}_{H_2}(L) \cdot r$$

$$\dot{n}_{H_2}(L) = (\dot{n}_{H_2})_{in} - \frac{W}{2F}\int_0^L i(x)dx = (\dot{n}_{H_2})_{in} - \frac{J}{2F} = (\dot{n}_{H_2})_{in} - 2\dot{n}_{O_2}$$

$$(\dot{n}_{H_2})_{in} = (3 + \varepsilon_{WGS})\dot{N}_{CH_4} + [(\dot{n}_{H_2})_{in} - 2\dot{n}_{O_2}] \cdot r$$

$$(\dot{n}_{H_2})_{in} = \frac{(3 + \varepsilon_{WGS})\dot{N}_{CH_4} - 2\dot{n}_{O_2} \cdot r}{(1-r)}$$

$$\dot{n}_{H_2}(x) = \frac{(3+\varepsilon_{WGS})\dot{N}_{CH_4} - 2\dot{n}_{O_2}\cdot r}{(1-r)} - \frac{W}{2F}\int_0^L i(x)dx$$

$$X_{H_2}(x) = 1 + \frac{\varepsilon_{WGS}}{3} - \frac{2\dot{n}_{O_2}\cdot r}{3\dot{N}_{CH_4}} - \frac{W(1-r)}{6F\dot{N}_{CH_4}}\int_0^x i(x)dx$$

$$(\dot{n}_{H_2O})_{in} = \dot{n}_{H_2O}(L)\cdot r - (1+\varepsilon_{WGS})\dot{N}_{CH_4}$$

$$\dot{n}_{H_2O}(L) = (\dot{n}_{H_2O})_{in} + \frac{W}{2F}\int_0^L i(x)dx = (\dot{n}_{H_2O})_{in} + 2\dot{n}_{O_2}$$

$$(\dot{n}_{H_2O})_{in} = ((\dot{n}_{H_2O})_{in} + 2\dot{n}_{O_2})r - (1+\varepsilon_{WGS})\dot{N}_{CH_4}$$

$$(\dot{n}_{H_2O})_{in} = \frac{2\dot{n}_{O_2}r - (1+\varepsilon_{WGS})\dot{N}_{CH_4}}{(1-r)}$$

$$\dot{n}_{H_2O}(x) = (\dot{n}_{H_2O})_{in} + \frac{W}{2F}\int_0^x i(x)dx$$

$$\dot{n}_{H_2O}(x) = \frac{2\dot{n}_{O_2}r - (1+\varepsilon_{WGS})\dot{N}_{CH_4}}{(1-r)} + \frac{W}{2F}\int_0^x i(x)dx$$

$$X_{H_2O}(x) = \frac{2\dot{n}_{O_2}r}{3\dot{N}_{CH_4}} - \frac{(1+\varepsilon_{WGS})}{3} + \frac{W(1-r)}{6F\dot{N}_{CH_4}}\int_0^x i(x)dx$$

$$\dot{n}_{CO}(L) = \varepsilon_{WGS}\cdot\dot{N}_{CH_4}$$

$$X_{CO}(L) = \frac{\varepsilon_{WGS}(1-r)}{3}$$

$$X_{CO_2}(L) = 1 - X_{CO}(L) - X_{H_2O}(L) - X_{H_2}(L)$$

Recirculation and Steam to Carbon Ratio:

$$S2C = \frac{\dot{n}_{H_2O}(L)\cdot r}{\dot{N}_{CH_4}}$$

$$S2C = \frac{\left[\frac{2\dot{n}_{O_2}r - (1+\varepsilon_{WGS})\dot{N}_{CH_4}}{(1-r)} + 2\dot{n}_{O_2}\right]r}{\dot{N}_{CH_4}}$$

Energy Balance:

$$\dot{Q}_{Gen} = \frac{-iA}{4F}(\Delta h_f^0)_{2H_2+O_2\rightarrow 2H_2O} - V\cdot\dot{n}_{O_2}\cdot 4F$$

$$\dot{Q}_{Reform} = \dot{N}_{CH_4}\cdot(\Delta h_f^0)_{CH_4+H_2O\rightarrow 3H_2+CO} + \dot{N}_{CH_4}\varepsilon_{WGS}\cdot(\Delta h_f^0)_{CO+H_2O\rightarrow H_2+CO_2}$$

10.3. Spreadsheet example for economic calculations

The following is an example of the spreadsheet used to calculate the costs from Chapter 6.

Totals	January	February	March	April	May	June	July	August	September	October	November	December
Total MWh	9,935.68	10,031.80	10,015.70	10,144.00	10,725.07	11,086.34	10,252.73	10,806.07	10,858.96	11,330.91	10,923.11	9,789.66
Grid Only Costs	553,043.46	559,666.91	559,041.30	566,834.08	594,985.05	616,702.94	582,217.21	614,997.94	608,990.33	641,187.27	612,371.72	549,167.96
Grid Emissions	4366.729665	4408.974266	4401.898348	4458.287986	4713.66835	4874.22645	4506.07293	4749.26991	4772.51127	4979.93288	4800.70879	4304.28879
Baseload Costs ($)	$187,530.98	$187,461.24	$187,461.24	$187,461.24	$187,461.24	$187,461.24	$187,461.24	$187,461.24	$187,461.24	$187,461.24	$187,461.24	$187,461.24
Grid/Demand Costs ($)	$186,918.53	$193,666.91	$192,848.09	$200,834.08	$228,985.05	$250,780.68	$216,217.21	$248,997.94	$242,990.33	$275,187.27	$246,261.26	$183,167.96
Total Costs ($)	$374,449.51	$381,128.14	$380,309.32	$388,295.31	$416,446.29	$438,241.91	$403,678.45	$436,459.17	$430,451.57	$462,648.51	$433,722.49	$370,629.19
Baseload Emissions (to	2,437.90	2,437.90	2,437.90	2,437.90	2,437.90	2,437.90	2,437.90	2,437.90	2,437.90	2,437.90	2,437.90	2,437.90
Grid/Demand Emission	1,412.19	1,455.53	1,446.76	1,504.85	1,760.23	1,919.00	1,552.63	1,795.83	1,819.07	2,026.49	1,847.27	1,349.12
Total Emissions (tons)	3,850.09	3,893.44	3,884.66	3,942.75	4,198.13	4,356.91	3,990.54	4,233.73	4,256.97	4,464.40	4,285.17	3,787.02
Peaker Costs ($)	$450,769.41	$453,630.56	$454,493.55	$458,410.36	$481,189.47	$496,410.21	$465,942.79	$486,687.13	$489,722.23	$510,959.30	$490,862.53	$446,511.81
Peaker Emissions (tons	5,860.00	5,897.20	5,908.42	5,959.33	6,255.46	6,453.33	6,057.26	6,326.93	6,366.39	6,642.47	6,347.96	5,804.65
dFC-GT Costs ($)	$258,866.77	$260,835.57	$260,362.93	$263,009.31	$274,422.92	$281,449.70	$264,917.90	$275,930.69	$276,886.39	$286,138.79	$278,216.35	$255,827.79
dFC-GT Emissions (tons	3,365.27	3,390.86	3,384.72	3,419.12	3,567.50	3,658.85	3,443.93	3,587.10	3,599.52	3,719.80	3,616.81	3,325.76

Total kWh (Annual)	Total MWh (Annual)	Total Effective Cos
125,900,013.20	125,900.01	13,106,191.37
National Average Effec	National Average Effective Cost ($/kWh	
10.41	0.1041	
(cents/kWh)	Our Assumption ($/kWh)	
5.61	0.0561	
Costs		
Grid Electric ($/MWh)	50	
Demand Charge ($/MW	3000	
Natural Gas ($/Mmbtu	4.5	

Annual Totals	Grid Only	Base + Grid	Peaker	dFC-GT
Fuel Costs ($)	$7,059,206.16	$4,916,459.88	$5,685,589.36	$3,236,865.12
Emissions (tons)	55,336.57	49,143.81	73,879.40	42,079.25
Mortgage Payment ($)	0	$953,825.21	$1,192,281.51	$2,384,563.02
Total Costs ($)	$7,059,206.16	$5,870,285.09	$6,877,870.87	$5,621,428.13